

Superiorization: An optimization heuristic for medical physics

Gabor T. Herman*

*Department of Computer Science, The Graduate Center,
City University of New York, New York, NY 10016, USA*

Edgar Garduño

*Departamento de Ciencias de la Computación,
Instituto de Investigaciones en Matemáticas Aplicadas y en Sistemas,
Universidad Nacional Autónoma de México,
Cd. Universitaria, C.P. 04510, Mexico City, Mexico*

Ran Davidi

Department of Radiation Oncology, Stanford University, Stanford, CA 94305, USA

Yair Censor

Department of Mathematics, University of Haifa, Mt. Carmel, 31905 Haifa, Israel

Purpose: To describe and mathematically validate the superiorization methodology, which is a recently-developed heuristic approach to optimization, and to discuss its applicability to medical physics problem formulations that specify the desired solution (of physically given or otherwise obtained constraints) by an optimization criterion.

Methods: The superiorization methodology is presented as a heuristic solver for a large class of constrained optimization problems. The constraints come from the desire to produce a solution that is constraints-compatible, in the sense of meeting requirements provided by physically or otherwise obtained constraints. The underlying idea is that many iterative algorithms for finding such a solution are perturbation resilient in the sense that, even if certain kinds of changes are made at the end of each iterative step, the algorithm still produces a constraints-compatible solution. This property is exploited by using permitted changes to steer the algorithm to a solution that is not only constraints-compatible, but is also desirable according to a specified optimization criterion. The approach is very general, it is applicable to

many iterative procedures and optimization criteria used in medical physics.

Results: The main practical contribution is a procedure for automatically producing from any given iterative algorithm its superiorized version, which will supply solutions that are superior according to a given optimization criterion. It is shown that if the original iterative algorithm satisfies certain mathematical conditions, then the output of its superiorized version is guaranteed to be as constraints-compatible as the output of the original algorithm, but it is superior to the latter according to the optimization criterion. This intuitive description is made precise in the paper and the stated claims are rigorously proved. Superiorization is illustrated on simulated computerized tomography data of a head cross-section and, in spite of its generality, superiorization is shown to be competitive to an optimization algorithm that is specifically designed to minimize total variation.

Conclusions: The range of applicability of superiorization to constrained optimization problems is very large. Its major utility is in the automatic nature of producing a superiorization algorithm from an algorithm aimed at only constraints-compatibility; while non-heuristic (exact) approaches need to be redesigned for a new optimization criterion. Thus superiorization provides a quick route to algorithms for the practical solution of constrained optimization problems.

Keywords: superiorization, constrained optimization, heuristic optimization, tomography, total variation

I. INTRODUCTION

Optimization is a tool that is used in many areas of Medical Physics. Prime examples are radiation therapy treatment planning and tomographic reconstruction, but there are others such as image registration. Some well-cited classical publications on the topic are¹⁻¹² and some recent articles are¹³⁻²⁶.

In a typical medical physics application, one uses *constrained optimization*, where the constraints come from the desire to produce a solution that is *constraints-compatible*, in the sense of meeting the requirements provided by physically or otherwise obtained constraints. In radiation therapy treatment planning, the requirements are usually in the form

of constraints prescribed by the treatment planner on the doses to be delivered at specific locations in the body. These doses in turn depend on information provided by an imaging instrument, typically a Magnetic Resonance Imaging (MRI) or a Computerized Tomography (CT) scanner. In tomography, the constraints come from the detector readings of the instrument. In such applications, it is typically the case that a large number of solutions would be considered good enough from the point of view of being constraints-compatible; to a large extent, but not entirely, due to the fact that there is uncertainty as to the exact nature of the constraints (for example, due to noise in the data collection). In such a case, an optimization criterion is introduced that helps us to distinguish the “better” constraints-compatible solutions (for example, this criterion could be the total dose to be delivered to the body, which may vary quite a bit between radiation therapy treatment plans that are compatible with the constraints on the doses delivered to individual locations).

The superiorization methodology (see, for example, ^{22,27–32}) is a recently-developed heuristic approach to optimization. The word *heuristic* is used here in the sense that the process is not guaranteed to lead to an optimum according to the given criterion; approaches aimed at processes that are guaranteed in that sense are usually referred to as *exact*. Heuristic approaches have been found useful in practical applications of optimization, mainly because they are often computationally much less expensive than their exact counterparts, but nevertheless provide solutions that are appropriate for the application at hand ^{33–35}.

The underlying idea of the superiorization approach is the following. In many applications there exists a computationally-efficient iterative algorithm that produces a constraints-compatible solution for the given constraints. (An example of this for radiation therapy treatment planning is reported in ³⁶, its clinical use is discussed in ¹⁵.) Furthermore, often the algorithm is *perturbation resilient* in the sense that, even if certain kinds of changes are made at the end of each iterative step, the algorithm still produces a constraints-compatible solution ^{27–30}. This property is exploited in the superiorization approach by using such perturbations to steer the algorithm to a solution that is not only constraints-compatible, but is also desirable according to a specified optimization criterion. The approach is very general, it is applicable to many iterative procedures and optimization criteria.

The current paper presents a major advance in the practice and theory of superiorization. The previous publications ^{22,27–32} used the intuitive idea to present some superiorization algorithms, in this paper the reader will find a totally automatic procedure that turns an

90 iterative algorithm into its superiorized version. This version will produce an output that
 91 is as constraints-compatible as the output of the original algorithm, but it is superior to
 92 that according to an optimization criterion. This claim is mathematically shown to be
 93 true for a very large class of iterative algorithms and for optimization criteria in general,
 94 typical restrictions (such as convexity) on the optimization criterion are not essential for
 95 the material presented below. In order to make precise and validate this broad claim, we
 96 present here a new theoretical framework. The framework of²⁹ is a precursor of what we
 97 present here, but it is a restricted one, since it assumes that the constraints can be all
 98 satisfied simultaneously, which is often false in medical physics applications. There is no
 99 such restriction in the presentation below.

100 The idea of designing algorithms that use interlacing steps of two different kinds (in our
 101 case, one kind of steps aim at constraints-compatibility and the other kind of steps aim at
 102 improvement of the optimization criterion) is well-established and, in fact, is made use of
 103 in many approaches that have been proposed with exact constrained optimization in mind;
 104 see, for example, the works of Helou Neto and De Pierro^{37,38}, of Nurminski³⁹, of Combettes
 105 and coworkers^{40,41}, of Sidky and Pan and coworkers^{23,42,43} and of Defrise and coworkers⁴⁴.
 106 However, none of these approaches can do what can be done by the superiorization approach
 107 as presented below, namely the automatic production of a heuristic constrained optimization
 108 algorithm from an iterative algorithm for constraints-compatibility. For example, in³⁷ it is
 109 assumed (just as in the theory presented in our²⁹) that all the constraints can be satisfied
 110 simultaneously.

111 A major motivator for the additional theory presented in the current paper is to get rid
 112 of this assumption, which is not reasonable when handling real problems of medical physics.
 113 Motivated by similar considerations, Helou Neto and De Pierro³⁸ present an alternative
 114 approach that does not require this unreasonable assumption. However, in order to solve
 115 such a problem, they end up with iterative algorithms of a particular form rather than having
 116 the generality of being able to turn any constraints-compatibility seeking algorithm into a
 117 superiorized one capable of handling constrained optimization. Also, the assumptions they
 118 have to make in order to prove their convergence result (their Theorem 15) indicate that
 119 their approach is applicable to a smaller class of constrained optimization problems than
 120 the superiorization approach whose applicability seems to be more general. However, for
 121 the mathematical purist, we point out that they present an exact constrained optimization

algorithm, while superiorization is a heuristic approach. Whether this is relevant to medical physics practice is not clear: exact algorithms are not run forever, but are stopped according to some stopping-rule, the relevant questions in comparing two algorithms are the quality of the actual output and the computation time needed to obtain it.

Ultimately, the quality of the outputs should be evaluated by some figures of merit relevant to the medical task at hand. An example of a careful study of this kind that involves superiorization is in³⁰ (Section 4.3), which reports on comparing in CT the efficacy of constrained optimization reconstruction algorithms for the detection of low-contrast brain tumors by using the method of statistical hypothesis testing (which provides a P-value that indicates the significance by which we can reject the null hypothesis that the two algorithms are equally efficacious in favor of the alternative that one is preferable). Such studies bundle together two things: (i) the formulation of the constrained optimization task and (ii) the performance of the algorithm in performing that task. The first of these requires a translation of the medical aim into a mathematical model, it is important that this model should be appropriately chosen.

The superiorization approach is not about choosing this model, it kicks in once the model is chosen and aims at producing an output that is “good” according to the mathematical specifications of the constraints and of the optimization criterion. Thus superiorization has been used to compare the effects on the quality of the output in CT when the optimization criterion is specified by total variation (TV) versus by entropy²⁸ or versus by the ℓ_1 -norm of the Haar transform³². However, the current paper is not about discussing how to translate the underlying medical physics task into a constrained optimization problem. For our purposes here, we are assuming that the mathematical model has been worked out and concentrate on the algorithmic approach for solving the resulting constrained optimization problem. We claim that the evaluation of such algorithms should not be based on the medical figures of merit mentioned at the beginning of the previous paragraph, but rather on their performance in solving the mathematical problem. If “good” solutions to the constrained optimization problem are not medically efficacious, that indicates that something is wrong with the mathematical model and not that something is wrong with the algorithmic approach. For this reason, in this paper we will not carry out a careful investigation of the medical efficacy of any algorithm in the manner that we have done in³⁰ (Section 4.3), but will restrict ourselves to a simple illustration of the performance of the superiorization approach

as compared to the previously published algorithm of⁴² that is aimed at performing exact minimization.

Examples of such studies already exist. Superiorization was compared in²⁷ with Algorithm 6 of⁴⁰ and in⁴⁵ with the algorithm of Goldstein and Osher that they refer to as TwIST⁴⁶ with split Bregman⁴⁷ as the substep. In both cases the implementation was done by the proposers of the algorithms. In these reported instances superiorization did well: the constraints-compatibility and the value of the function to be minimized were very similar for the outputs produced by the algorithms being compared, but the superiorization algorithm produced its output four times faster than the alternative. It would be unjustified to draw any general conclusions on the mathematical performance and speed of superiorization based on just a few experiments, but the reported results are encouraging.

However, the main reason why we advocate superiorization is different from what is discussed above. The reason why we claim it to be helpful in medical physics research is that it has the potential of saving a lot of time and effort for the researcher. Let us consider a historical example. Likelihood optimization using the iterative process of expectation maximization (EM)⁴⁸ gained immediate and wide acceptance in the emission tomography community. It was observed that irregular high amplitude patterns occurred in the image with a large number of iterations, but it was not until five years later that this problem was corrected⁴⁹ by the use of a maximum a posteriority probability (MAP) algorithm with a multivariate Gaussian prior. Had we had at our disposal the superiorization approach, then the introduction of an optimization criterion (Gaussian or other) into the iterative expectation maximization (EM) process would have been a simple matter and we would have saved the time and effort spent on designing a special purpose algorithm for the MAP formulation. A *TV*-superiorization of the EM algorithm is presented in⁵⁰.

Even though our major claim for superiorization is that it provides a quick route to algorithms for the practical solution of constrained optimization problems, before leaving this introduction let us bring up a question that has to do with the performance of the resulting algorithms: Will superiorization produce superior results to those produced by contemporary MAP methods or is it faster than the better of such methods? At this stage we have not yet developed the mathematical notation to discuss this question in a rigorous manner, we return to it in Subsection **II F**.

In the next section we present in detail the superiorization methodology. In the subse-

quent section we provide an illustrative example by reporting on reconstructions produced by algorithms applied to simulated computerized tomography data of a head cross-section. In the final section we discuss our results and present our conclusions.

II. THE SUPERIORIZATION METHODOLOGY

A. Problem sets, proximity functions and ε -compatibility

Although optimization is often studied in a more general context (such as in Hilbert or Banach spaces), in medical physics we usually deal with a special case, where optimization is performed in a *Euclidean space* \mathbb{R}^J (the space of J -dimensional vectors of real numbers, where J is a positive integer). As often appropriate in practice, we further restrict the domain of optimization to a nonempty subset Ω of \mathbb{R}^J (such as the *nonnegative orthant* \mathbb{R}_+^J that consists of vectors all of whose components are nonnegative).

We now turn to formalizing the notion of being compatible with given constraints, a notion that we have used informally in the previous section. In any application, there is a *problem set* \mathbb{T} ; each *problem* $T \in \mathbb{T}$ is essentially a description of the constraints in that particular case. For example, for a tomographic scanner, the problem of reconstruction for a particular patient at a particular time is determined by the measurements taken by the scanner for that patient at that time. The intuitive notion of constraints-compatibility is formalized by the use of a *proximity function* $\mathcal{P}r$ on \mathbb{T} such that, for every $T \in \mathbb{T}$, $\mathcal{P}r_T$ maps Ω into \mathbb{R}_+ , the set of nonnegative real numbers; i.e., $\mathcal{P}r_T : \Omega \rightarrow \mathbb{R}_+$. Intuitively we think of $\mathcal{P}r_T(\mathbf{x})$ as an indicator of how incompatible \mathbf{x} is with the constraints of T . For example, in tomography, $\mathcal{P}r_T(\mathbf{x})$ should indicate by how much a proposed reconstruction that is described by an \mathbf{x} in Ω violates the constraints of the problem T that are provided by the measurements taken by the scanner. For example, if we use \mathbf{b} to denote the vector of estimated line integrals based on the measurements obtained by the scanner and by \mathbf{A} the system matrix of the scanner, then a possible choice for the proximity function is the norm-distance $\|\mathbf{b} - \mathbf{A}\mathbf{x}\|$, which we will use as an example in the discussions that follow. An alternative legitimate choice for the proximity function is the Kullback-Leibler distance $KL(\mathbf{b}, \mathbf{A}\mathbf{x})$, which is the negative log-likelihood of a statistical model in tomography. The special case $\mathcal{P}r_T(\mathbf{x}) = 0$ is interpreted by saying that \mathbf{x} is perfectly compatible with the

constraints; due to the presence of noise in practical applications, it is quite conceivable that there is no \mathbf{x} that is perfectly compatible with the constraints, and we accept an \mathbf{x} as constraints-compatible as long as the value of $\mathcal{P}r_T(\mathbf{x})$ is considered to be small enough to justify that decision. Combining these two concepts leads to the notion of a *problem structure*, which is a pair $\langle \mathbb{T}, \mathcal{P}r \rangle$, where \mathbb{T} is a nonempty problem set and $\mathcal{P}r$ is a proximity function on \mathbb{T} . For a problem structure $\langle \mathbb{T}, \mathcal{P}r \rangle$, a problem $T \in \mathbb{T}$, a nonnegative ε and an $\mathbf{x} \in \Omega$, we say that \mathbf{x} is ε -compatible with T provided that $\mathcal{P}r_T(\mathbf{x}) \leq \varepsilon$.

As an example (whose applicability to tomographic reconstruction is illustrated in Section III), consider the problem structure that arises from the desire to find nonnegative solutions of sequences of blocks of linear equations. Then the appropriate choices are $\Omega = \mathbb{R}_+^J$ and the problem structure is $\langle \mathbb{S}, Res \rangle$, where the problem set \mathbb{S} is

$$\begin{aligned} \mathbb{S} = & \left\{ \left(\{(\mathbf{a}^1, b_1), \dots, (\mathbf{a}^{\ell_1}, b_{\ell_1})\}, \dots, \right. \right. \\ & \left. \left. \{(\mathbf{a}^{\ell_1+\dots+\ell_{W-1}+1}, b_{\ell_1+\dots+\ell_{W-1}+1}), \dots, (\mathbf{a}^{\ell_1+\dots+\ell_W}, b_{\ell_1+\dots+\ell_W})\} \right) \right\} \\ & W \text{ is a positive integer and,} \\ & \text{for } 1 \leq w \leq W, \ell_w \text{ is a positive integer and,} \\ & \text{for } 1 \leq i \leq \ell_1 + \dots + \ell_W, \mathbf{a}^i \in \mathbb{R}^J \text{ and } b_i \in \mathbb{R} \end{aligned} \quad (1)$$

and the proximity function Res on \mathbb{S} is defined, for any problem $S = (\{(\mathbf{a}^1, b_1), \dots, (\mathbf{a}^{\ell_1}, b_{\ell_1})\}, \dots, \{(\mathbf{a}^{\ell_1+\dots+\ell_{W-1}+1}, b_{\ell_1+\dots+\ell_{W-1}+1}), \dots, (\mathbf{a}^{\ell_1+\dots+\ell_W}, b_{\ell_1+\dots+\ell_W})\})$ in \mathbb{S} and for any $\mathbf{x} \in \Omega$, by

$$Res_S(\mathbf{x}) = \sqrt{\sum_{i=1}^{\ell_1+\dots+\ell_W} (b_i - \langle \mathbf{a}^i, \mathbf{x} \rangle)^2}. \quad (2)$$

Note that each element of this problem set \mathbb{S} specifies an ordered sequence of W blocks of linear equations of the form $\langle \mathbf{a}^i, \mathbf{x} \rangle = b_i$ where $\langle *, * \rangle$ denotes the inner product in \mathbb{R}^J (and thus \mathbb{S} is an appropriate representation of the so-called “ordered subsets” approach to tomographic reconstruction⁵¹, as well as of other earlier-published block-iterative methods that proposed essentially the same idea^{52–54}). The proximity function Res on \mathbb{S} is the *residual* that we get when a particular \mathbf{x} is substituted into all the equations of a particular problem S .

B. Algorithms and outputs

We now define the concept of an algorithm in the general context of problem structures. For technical reasons that will become clear as we proceed with our development, we introduce an additional set Δ , such that $\Omega \subseteq \Delta \subseteq \mathbb{R}^J$. (Both Ω and Δ are assumed to be known and fixed for any particular problem structure $\langle \mathbb{T}, \mathcal{P}r \rangle$.) An *algorithm* \mathbf{P} for a problem structure $\langle \mathbb{T}, \mathcal{P}r \rangle$ assigns to each problem $T \in \mathbb{T}$ an operator $\mathbf{P}_T : \Delta \rightarrow \Omega$. This definition is used to define iterative processes that, for any *initial point* $\mathbf{x} \in \Omega$, produce the (potentially) infinite sequence $\left((\mathbf{P}_T)^k \mathbf{x} \right)_{k=0}^{\infty}$ (that is, the sequence $\mathbf{x}, \mathbf{P}_T \mathbf{x}, \mathbf{P}_T (\mathbf{P}_T \mathbf{x}), \dots$) of points in Ω . We discuss below how such a potentially infinite process is terminated in practice.

Selecting $\Omega = \mathbb{R}_+^J$ and $\Delta = \mathbb{R}^J$ for the problem structure $\langle \mathbb{S}, Res \rangle$ of the previous subsection, an example of an algorithm \mathbf{R} is specified by

$$\mathbf{R}_S \mathbf{x} = \mathbf{Q} \mathbf{B}_{S_W} \cdots \mathbf{B}_{S_1} \mathbf{x}, \quad (3)$$

where S is the problem specified above (2) and, for $1 \leq w \leq W$, $\mathbf{B}_{S_w} : \Delta \rightarrow \Delta$ is defined by

$$\mathbf{B}_{S_w} \mathbf{x} = \mathbf{x} + \frac{1}{\ell_w} \sum_{i=\ell_1+\dots+\ell_{w-1}+1}^{\ell_1+\dots+\ell_w} \frac{b_i - \langle \mathbf{a}^i, \mathbf{x} \rangle}{\|\mathbf{a}^i\|^2} \mathbf{a}^i, \quad (4)$$

where $\|\mathbf{a}\|$ denotes the norm of the vector \mathbf{a} in \mathbb{R}^J , and $\mathbf{Q} : \Delta \rightarrow \Omega$ is defined by

$$(\mathbf{Q}\mathbf{x})_j = \max \{0, x_j\}, \text{ for } 1 \leq j \leq J. \quad (5)$$

Note that $\mathbf{R}_S : \Delta \rightarrow \Omega$. This specific algorithm \mathbf{R} is a typical example of the so-called block-iterative methods mentioned above. Except for the presence of \mathbf{Q} in (3), which enforces nonnegativity of the components, it is identical to an algorithm used and illustrated in³¹. With the \mathbf{Q} absent from the definition of the algorithm, Ω has to be the whole of \mathbb{R}^J ; the practical consequence of the presence versus the absence of \mathbf{Q} in the tomographic application is illustrated in Subsection IIID. We note also that special cases of the presented algorithm include the classical reconstruction methods ART (if $\ell_w = 1$, for $1 \leq w \leq W$) and SIRT (if $W = 1$); see, for example, Chapters 11 and 12 of⁵⁵.

For a problem structure $\langle \mathbb{T}, \mathcal{P}r \rangle$, a $T \in \mathbb{T}$, an $\varepsilon \in \mathbb{R}_+$ and a sequence $R = (\mathbf{x}^k)_{k=0}^{\infty}$ of points in Ω , we use $O(T, \varepsilon, R)$ to denote the $\mathbf{x} \in \Omega$ that has the following properties: $\mathcal{P}r_T(\mathbf{x}) \leq \varepsilon$ and there is a nonnegative integer K such that $\mathbf{x}^K = \mathbf{x}$ and, for all nonnegative integers $k < K$, $\mathcal{P}r_T(\mathbf{x}^k) > \varepsilon$. Clearly, if there is such an \mathbf{x} , then it is unique. If there is no

such \mathbf{x} , then we say that $O(T, \varepsilon, R)$ is *undefined*, otherwise we say that it is *defined*. The intuition behind this definition is the following: if we think of R as the (infinite) sequence of points that is produced by an algorithm (intended for the problem T) without a termination criterion, then $O(T, \varepsilon, R)$ is the *output* produced by that algorithm when we add to it instructions that make it terminate as soon as it reaches a point that is ε -compatible with T .

C. Bounded perturbation resilience

The notion of a *bounded perturbations resilient* algorithm \mathbf{P} for a problem structure $\langle \mathbb{T}, \mathcal{Pr} \rangle$ has been defined in a mathematically precise manner²⁹. However, that definition is not satisfactory from the point of view of applications in medical physics (or indeed in any area involving noisy data), because it is useful only for problems T for which there is a perfectly compatible solution (that is, an \mathbf{x} such that $\mathcal{Pr}_T(\mathbf{x}) = 0$). We therefore extend here that notion as follows. An algorithm \mathbf{P} for a problem structure $\langle \mathbb{T}, \mathcal{Pr} \rangle$ is said to be *strongly perturbation resilient* if, for all $T \in \mathbb{T}$,

- (i) there exists an $\varepsilon \in \mathbb{R}_+$ such that $O\left(T, \varepsilon, \left((\mathbf{P}_T)^k \mathbf{x}\right)_{k=0}^{\infty}\right)$ is defined for every $\mathbf{x} \in \Omega$;
- (ii) for all $\varepsilon \in \mathbb{R}_+$ such that $O\left(T, \varepsilon, \left((\mathbf{P}_T)^k \mathbf{x}\right)_{k=0}^{\infty}\right)$ is defined for every $\mathbf{x} \in \Omega$, we also have that $O(T, \varepsilon', R)$ is defined for every $\varepsilon' > \varepsilon$ and for every sequence $R = (\mathbf{x}^k)_{k=0}^{\infty}$ of points in Ω generated by

$$\mathbf{x}^{k+1} = \mathbf{P}_T(\mathbf{x}^k + \beta_k \mathbf{v}^k), \text{ for all } k \geq 0, \quad (6)$$

where $\beta_k \mathbf{v}^k$ are *bounded perturbations*, meaning that the sequence $(\beta_k)_{k=0}^{\infty}$ of nonnegative real numbers is *summable* (that is, $\sum_{k=0}^{\infty} \beta_k < \infty$), the sequence $(\mathbf{v}^k)_{k=0}^{\infty}$ of vectors in \mathbb{R}^J is bounded and, for all $k \geq 0$, $\mathbf{x}^k + \beta_k \mathbf{v}^k \in \Delta$.

In less formal terms, the second of these properties says that for a strongly perturbation resilient algorithm we have that, for every problem and any nonnegative real number ε , if it is the case that for all initial points from Ω the infinite sequence produced by the algorithm contains an ε -compatible point, then it will also be the case that all perturbed sequences satisfying (6) contain an ε' -compatible point, for any $\varepsilon' > \varepsilon$.

287 Having defined the notion of a strongly perturbation resilient algorithm, we next show
 288 that this notion is of relevance to problems in medical physics. We illustrate the use of this
 289 in tomography in the next section. We first need to introduce some mathematical concepts.

290 Given an algorithm \mathbf{P} for a problem structure $\langle \mathbb{T}, \mathcal{Pr} \rangle$ and a $T \in \mathbb{T}$, we say that
 291 \mathbf{P} is *convergent for T* if, for every $\mathbf{x} \in \Omega$, there exists a unique $\mathbf{y}(\mathbf{x}) \in \Omega$ such that,
 292 $\lim_{k \rightarrow \infty} (\mathbf{P}_T)^k \mathbf{x} = \mathbf{y}(\mathbf{x})$, meaning that for every positive real number δ , there exist a non-
 293 negative integer K , such that $\|(\mathbf{P}_T)^k \mathbf{x} - \mathbf{y}(\mathbf{x})\| \leq \delta$, for all nonnegative integers $k \geq K$.
 294 If, in addition, there exists a $\gamma \in \mathbb{R}_+$ such that $\mathcal{Pr}_T(\mathbf{y}(\mathbf{x})) \leq \gamma$, for every $\mathbf{x} \in \Omega$, then we
 295 say that \mathbf{P} is *boundedly convergent for T* .

296 A function $f : \Omega \rightarrow \mathbb{R}$ is *uniformly continuous* if, for every $\varepsilon > 0$ there exists a $\delta > 0$,
 297 such that, for all $\mathbf{x}, \mathbf{y} \in \Omega$, $|f(\mathbf{x}) - f(\mathbf{y})| \leq \varepsilon$ provided that $\|\mathbf{x} - \mathbf{y}\| \leq \delta$. An example of a
 298 uniformly continuous function is Res_S of (2), for any $S \in \mathbb{S}$. This can be proved by observing
 299 that the right-hand side of (2) can be rewritten in vector/matrix form as $\|\mathbf{b} - \mathbf{A}\mathbf{x}\|$ and
 300 then selecting, for any given $\varepsilon > 0$, δ to be $\varepsilon / \|\mathbf{A}\|$, where $\|\mathbf{A}\|$ denotes the matrix norm of
 301 \mathbf{A} .

302 An operator $\mathbf{O} : \Delta \rightarrow \Omega$, is *nonexpansive* if $\|\mathbf{O}\mathbf{x} - \mathbf{O}\mathbf{y}\| \leq \|\mathbf{x} - \mathbf{y}\|$, for all $\mathbf{x}, \mathbf{y} \in \Delta$.
 303 An example of a nonexpansive operator is the \mathbf{R}_S of (3). The proof of this is also simple.
 304 It follows from discussions regarding similar claims in²⁷ that the $\mathbf{B}_{S_w} : \mathbb{R}^J \rightarrow \mathbb{R}^J$ of (4) is a
 305 nonexpansive operator, for $1 \leq w \leq W$, and that the operator \mathbf{Q} of (5) is also nonexpansive.
 306 Obviously, a sequential application of nonexpansive operators results in a nonexpansive
 307 operator and thus \mathbf{R}_S is nonexpansive.

308 Now we state an important new result that gives sufficient conditions for strong perturba-
 309 tion resilience: If \mathbf{P} is an algorithm for a problem structure $\langle \mathbb{T}, \mathcal{Pr} \rangle$ such that,
 310 for all $T \in \mathbb{T}$, \mathbf{P} is boundedly convergent for T , $\mathcal{Pr}_T : \Omega \rightarrow \mathbb{R}$ is uniformly
 311 continuous and $\mathbf{P}_T : \Delta \rightarrow \Omega$ is nonexpansive, then \mathbf{P} is strongly perturbation
 312 resilient. The importance of this result lies in the fact that the rather ordinary condition
 313 of uniform continuity for the proximity function and the reasonable conditions of bounded
 314 convergence and nonexpansiveness of the algorithmic operators guarantee that we end up
 315 with a strongly perturbation resilient algorithm. The proof of this new result involves some
 316 mathematical technicalities and is therefore presented in the Appendix as Theorem 1.

D. Optimization criterion and nonascending vector

Now suppose, as is indeed the case for the constrained optimization problems discussed in the previous section, that in addition to a problem structure $\langle \mathbb{T}, \mathcal{Pr} \rangle$ we are also provided with an optimization criterion, which is specified by a function $\phi : \Delta \rightarrow \mathbb{R}$, with the convention that a point in Δ for which the value of ϕ is smaller is considered *superior* (from the point of view of our application) to a point in Δ for which the value of ϕ is larger. In the tomography context, any of the functions of \mathbf{x} that are listed as a “secondary optimization criterion” (an alternative name is a “regularizer”) in Section 6.4 of⁵⁵ is an acceptable choice for the optimization criterion ϕ . These include weighted norms, the negative of Shannon’s entropy and total variation. It is the last of these that we discuss in detail in the illustrative example below. The essential idea of the *superiorization methodology* presented in this paper is to make use of the perturbations of (6) to transform a strongly perturbation resilient algorithm that seeks a constraints-compatible solution into one whose outputs are equally good from the point of view of constraints-compatibility, but are superior according to the optimization criterion. We do this by producing from the algorithm another one, called its *superiorized* version, by making sure not only that the $\beta_k \mathbf{v}^k$ are bounded perturbations, but also that $\phi(\mathbf{x}^k + \beta_k \mathbf{v}^k) \leq \phi(\mathbf{x}^k)$, for all $k \geq 0$.

In order to ensure this we introduce a new concept (closely related to the concept of a “descent direction” that is widely used in optimization). Given a function $\phi : \Delta \rightarrow \mathbb{R}$ and a point $\mathbf{x} \in \Delta$, we say that a vector $\mathbf{d} \in \mathbb{R}^J$ is *nonascending* for ϕ at \mathbf{x} if $\|\mathbf{d}\| \leq 1$ and

$$\begin{aligned} &\text{there is a } \delta > 0 \text{ such that for all } \lambda \in [0, \delta], \\ &(\mathbf{x} + \lambda \mathbf{d}) \in \Delta \text{ and } \phi(\mathbf{x} + \lambda \mathbf{d}) \leq \phi(\mathbf{x}). \end{aligned} \tag{7}$$

Note that irrespective of the choices of ϕ and \mathbf{x} , there is always at least one nonascending vector \mathbf{d} for ϕ at \mathbf{x} , namely the zero-vector, all of whose components are zero. This is a useful fact for proving results concerning the guaranteed behavior of our proposed procedures. However, in order to steer our algorithms toward a point at which the value of ϕ is small, we need to find a \mathbf{d} such that $\phi(\mathbf{x} + \lambda \mathbf{d}) < \phi(\mathbf{x})$ rather than just $\phi(\mathbf{x} + \lambda \mathbf{d}) \leq \phi(\mathbf{x})$ as in (7). In some earlier papers on superiorization^{27–31} it was assumed that $\Delta = \mathbb{R}^J$ and that ϕ is a convex function. This implied that, for any point $\mathbf{x} \in \Delta$, ϕ had a subgradient $\mathbf{g} \in \mathbb{R}^J$ at the point \mathbf{x} . It was suggested that if there is such a \mathbf{g} with a positive norm, then \mathbf{d} should be chosen to be $-\mathbf{g}/\|\mathbf{g}\|$, otherwise \mathbf{d} should be chosen to be the zero vector. However,

there are approaches (not involving subgradients) to selecting an appropriate \mathbf{d} ; an example can be found in³² in which \mathbf{d} is found without using subgradients for the case when ϕ is the ℓ_1 -norm of the Haar transform. The method we used for selecting a nonascending vector in the experiments reported in this paper is specified at the end of Subsection III A.

E. Superiorized version of an algorithm

We now make precise the ingredients needed for transforming an algorithm into its superiorized version. Let Ω and Δ be the underlying sets for a problem structure $\langle \mathbb{T}, \mathcal{P}r \rangle$ ($\Omega \subseteq \Delta \subseteq \mathbb{R}^J$, as discussed at the beginning of Subsection II B), \mathbf{P} be an algorithm for $\langle \mathbb{T}, \mathcal{P}r \rangle$ and $\phi : \Delta \rightarrow \mathbb{R}$. The following description of the Superiorized Version of Algorithm \mathbf{P} produces, for any problem $T \in \mathbb{T}$, a sequence $R_T = (\mathbf{x}^k)_{k=0}^\infty$ of points in Ω for which, for all $k \geq 0$, (6) is satisfied. We show this to be true, for any algorithm \mathbf{P} , after the description of the Superiorized Version of Algorithm \mathbf{P} . Furthermore, since the sequence R_T is steered by Superiorized Version of Algorithm \mathbf{P} toward a reduced value of ϕ , there is an intuitive expectation that the output of the superiorized version is likely to be superior (from the point of view of the optimization criterion ϕ) to the output of the original unperturbed algorithm. This last statement is not precise and so it cannot be proved in a mathematical sense for an arbitrary algorithm \mathbf{P} ; however, that should not stop us from applying the easy procedure given below for automatically producing the Superiorized Version of \mathbf{P} and experimentally checking whether it indeed provides us with outputs superior to those of the original algorithm. The well-demonstrated nature of heuristic optimization approaches is that they often work in practice even when their performance cannot be guaranteed to be optimal^{33–35}.

Nevertheless, we can push our theory further than the hope expressed in the last paragraph, by considering superiorized versions of algorithms that satisfy some condition. In this paper, the condition that we discuss is strong perturbation resilience. We show below that if \mathbf{P} is strongly perturbation resilient, then, for any problem $T \in \mathbb{T}$, a sequence R_T produced by its superiorized version has the following desirable property: For all $\varepsilon \in \mathbb{R}_+$, if $O(T, \varepsilon, ((\mathbf{P}_T)^k \mathbf{x})_{k=0}^\infty)$ is defined for every $\mathbf{x} \in \Omega$, then $O(T, \varepsilon', R_T)$ is also defined for every $\varepsilon' > \varepsilon$; in other words, the Superiorized Version of Algorithm \mathbf{P} provides an ε' -compatible output. As stated above, the advantage of the superiorized version is that its output is

likely to be superior to the output of the original unperturbed algorithm. We point out that strong perturbation resilience is a sufficient, but not necessary, condition for guaranteeing such desirable behavior of the superiorized version, finding additional sufficient conditions and proving that algorithms that we wish to superiorize satisfy such conditions is part of our ongoing research.

The superiorized version assumes that we have available a summable sequence $(\gamma_\ell)_{\ell=0}^\infty$ of positive real numbers (for example, $\gamma_\ell = a^\ell$, where $0 < a < 1$) and it generates, simultaneously with the sequence $(\mathbf{x}^k)_{k=0}^\infty$, sequences $(\mathbf{v}^k)_{k=0}^\infty$ and $(\beta_k)_{k=0}^\infty$. The latter is generated as a subsequence of $(\gamma_\ell)_{\ell=0}^\infty$, resulting in a summable sequence $(\beta_k)_{k=0}^\infty$. The algorithm further depends on a specified initial point $\bar{\mathbf{x}} \in \Omega$ and on a positive integer N . It makes use of a logical variable called *loop*.

Superiorized Version of Algorithm P

```

(i) set  $k = 0$ 

(ii) set  $\mathbf{x}^k = \bar{\mathbf{x}}$ 

(iii) set  $\ell = -1$ 

(iv) repeat

(v)     set  $n = 0$ 

(vi)    set  $\mathbf{x}^{k,n} = \mathbf{x}^k$ 

(vii)   while  $n < N$ 

(viii)      set  $\mathbf{v}^{k,n}$  to be a nonascending vector for  $\phi$  at  $\mathbf{x}^{k,n}$ 

(ix)      set  $loop = true$ 

(x)      while  $loop$ 

(xi)         set  $\ell = \ell + 1$ 

(xii)        set  $\beta_{k,n} = \gamma_\ell$ 

(xiii)       set  $\mathbf{z} = \mathbf{x}^{k,n} + \beta_{k,n} \mathbf{v}^{k,n}$ 

(xiv)       if  $\mathbf{z} \in \Delta$  and  $\phi(\mathbf{z}) \leq \phi(\mathbf{x}^k)$  then

```

402 (xv) **set** $n = n + 1$

403 (xvi) **set** $\mathbf{x}^{k,n} = \mathbf{z}$

404 (xvii) **set** $loop = false$

405 (xviii) **set** $\mathbf{x}^{k+1} = \mathbf{P}_T \mathbf{x}^{k,N}$

406 (xix) **set** $k = k + 1$

407 Next we analyze the behavior of the Superiorized Version of Algorithm **P**.

408 The iteration number k is set to 0 in (i) and $\mathbf{x}^k = \mathbf{x}^0$ is set to its initial value $\bar{\mathbf{x}}$ in (ii). The
 409 integer index ℓ for picking the next element from the sequence $(\gamma_\ell)_{\ell=0}^\infty$ is initialized to -1 by
 410 line (iii), it is repeatedly increased by line (xi). The lines (v) - (xix) that follow the **repeat**
 411 in (iv) perform a complete iterative step from \mathbf{x}^k to \mathbf{x}^{k+1} , infinite repetitions of such steps
 412 provide the sequence $R_T = (\mathbf{x}^k)_{k=0}^\infty$. During one iterative step, there is one application of
 413 the operator \mathbf{P}_T , in line (xviii), but there are N steering steps aimed at reducing the value of
 414 ϕ ; the latter are done by lines (v) - (xvii). These lines produce a sequence of points
 415 $\mathbf{x}^{k,n}$, where $0 \leq n \leq N$ with $\mathbf{x}^{k,0} = \mathbf{x}^k$, $\mathbf{x}^{k,n} \in \Delta$ and $\phi(\mathbf{x}^{k,n}) \leq \phi(\mathbf{x}^k)$.

416 We prove the truth of the last sentence by induction on the nonnegative integers. For
 417 $n = 0$, we have by lines (v) and (vi) that $\mathbf{x}^{k,0} = \mathbf{x}^k$. But $\mathbf{x}^k \in \Omega$, since it is either $\bar{\mathbf{x}}$ that is
 418 assumed to be in Ω due to lines (i) and (ii) or it is in the range Ω of \mathbf{P}_T due to lines (xviii)
 419 and (xix). Now we assume, for any $0 \leq n < N$, that $\mathbf{x}^{k,n} \in \Delta$ and $\phi(\mathbf{x}^{k,n}) \leq \phi(\mathbf{x}^k)$ and
 420 show that lines (viii) - (xvii) perform a computation that leads from $\mathbf{x}^{k,n}$ to an $\mathbf{x}^{k,n+1} \in \Delta$
 421 that satisfies $\phi(\mathbf{x}^{k,n+1}) \leq \phi(\mathbf{x}^k)$. To see this, observe that line (viii) sets $\mathbf{v}^{k,n}$ to be a
 422 nonascending vector for ϕ at $\mathbf{x}^{k,n}$, which implies that (7) is satisfied with $\mathbf{x} = \mathbf{x}^{k,n}$ and
 423 $\mathbf{d} = \mathbf{v}^{k,n}$. Line (ix) sets $loop$ to *true*, and it remains *true* while searching for the desired
 424 $\mathbf{x}^{k,n+1}$, by repeatedly executing the loop sequence that follows line (x). In this sequence,
 425 line (xi) increases ℓ by 1 and line (xii) sets $\beta_{k,n}$ to γ_ℓ . Thus for the vector \mathbf{z} defined by line
 426 (xiii), $\mathbf{z} \in \Delta$ and $\phi(\mathbf{z}) \leq \phi(\mathbf{x}^{k,n})$, provided that $\beta_{k,n}$ is not greater than the δ in (7). Since
 427 $(\gamma_\ell)_{\ell=0}^\infty$ is a summable sequence of positive real numbers, there must be a positive integer L
 428 such that $\gamma_\ell \leq \delta$, for all $\ell \geq L$. This implies that if we applied lines (xi) - (xiii) often enough,
 429 we would reach a vector \mathbf{z} that satisfies $\mathbf{z} \in \Delta$ and $\phi(\mathbf{z}) \leq \phi(\mathbf{x}^{k,n})$. If the condition in line
 430 (xiv) is not satisfied when the process gets to it, then lines (xi) - (xiii) are again executed
 431 and eventually we get a vector \mathbf{z} for which the condition in line (xiv) is satisfied due to the

induction hypothesis that $\phi(\mathbf{x}^{k,n}) \leq \phi(\mathbf{x}^k)$. By lines (xv) and (xvi) we see that at that time $\mathbf{x}^{k,n+1}$ is set to \mathbf{z} and so we obtain that $\mathbf{x}^{k,n+1} \in \Delta$ and $\phi(\mathbf{x}^{k,n+1}) \leq \phi(\mathbf{x}^k)$, as desired. Line (xvii) sets *loop* to *false* and so control is returned to line (vii). When this happens for the N th time, it will be the case that $n = N$ and therefore line (xviii) is used to produce $\mathbf{x}^{k+1} \in \Omega$ and the increasing of k by line (xix) allows us then to move on to the next iterative step. Infinite repetition of such steps produces the sequence $R_T = (\mathbf{x}^k)_{k=0}^\infty$ of points in Ω . We now show that if $O\left(T, \varepsilon, \left((\mathbf{P}_T)^k \mathbf{x}\right)_{k=0}^\infty\right)$ is defined for every $\mathbf{x} \in \Omega$, then, for any $\varepsilon' > \varepsilon$, the Superiorized Version of Algorithm **P** produces an ε' -compatible output. Since **P** is assumed to be strongly perturbation resilient, this desired result follows if we can show that there exists a summable sequence $(\beta_k)_{k=0}^\infty$ of nonnegative real numbers and a bounded sequence $(\mathbf{v}^k)_{k=0}^\infty$ of vectors in \mathbb{R}^J such that (6) is satisfied for all $k \geq 0$. In view of line (xviii), this is achieved if we can define the β_k and the \mathbf{v}^k so that $\mathbf{x}^{k,N} = \mathbf{x}^k + \beta_k \mathbf{v}^k$. This is done by setting

$$\beta_k = \max \{ \beta_{k,n} \mid 0 \leq n < N \}, \quad (8)$$

$$\mathbf{v}^k = \sum_{n=0}^{N-1} \frac{\beta_{k,n}}{\beta_k} \mathbf{v}^{k,n}. \quad (9)$$

That these assignments result in $\mathbf{x}^{k,N} = \mathbf{x}^k + \beta_k \mathbf{v}^k$ follows from lines (v) - (xvii). From line (xii) follows that $(\beta_k)_{k=0}^\infty$ is a subsequence of $(\gamma_\ell)_{\ell=0}^\infty$ and, hence, it is a summable sequence of nonnegative real numbers. Since each $\|\mathbf{v}^{k,n}\| \leq 1$ by the definition of a nonascending vector, it follows from (8) and (9) that $\|\mathbf{v}^k\| \leq N$ and so $(\mathbf{v}^k)_{k=0}^\infty$ is bounded. Part of the condition expressed in (6) is that, for all $k \geq 0$, $\mathbf{x}^k + \beta_k \mathbf{v}^k \in \Delta$. This follows from the fact that $\mathbf{x}^{k,N} = \mathbf{x}^k + \beta_k \mathbf{v}^k$ is assigned its value by line (xvi), but only if the condition expressed in line (xiv) is satisfied.

In conclusion, we have shown that the superiorized version of a strongly perturbation resilient algorithm produces outputs that are essentially as constraints-compatible as those produced by the original version of the algorithm. However, due to the repeated steering of the process by lines (vii) - (xvii) toward reducing the value of the optimization criterion ϕ , we can expect that the output of the superiorized version will be superior (from the point of view of ϕ) to the output of the original algorithm.

F. Information on performance comparison with MAP methods

Using our notation, the constrained minimization formulation that we are considering is:

Given an $\varepsilon \in \mathbb{R}_+$,

$$\text{minimize } \phi(\mathbf{x}), \text{ subject to } \mathcal{P}r_T(\mathbf{x}) \leq \varepsilon. \quad (10)$$

The aim of superiorization is not identical with the aim of constrained minimization in (10). One difference is that ε is not “given” in the superiorization context. The superiorization of an algorithm produces a sequence and, for any ε , the associated output of the algorithm is considered to be the first \mathbf{x} in the sequence for which $\mathcal{P}r_T(\mathbf{x}) \leq \varepsilon$. The other difference is that we do not claim that this output is a minimizer of ϕ among all points that satisfy the constraint, but hope only that it is usually an \mathbf{x} for which $\phi(\mathbf{x})$ is at the small end of its range of values over the set of constraint-satisfying points. This latter difference is generally shared by comparisons of a heuristic approach with an exact approach to solving a constrained minimization problem.

The MAP (or regularized) formulation of a physical problem that leads to the constrained minimization problem (10) is the unconstrained minimization problem of the form: Given a $\beta \in \mathbb{R}_+$,

$$\text{minimize } [\phi(\mathbf{x}) + \beta \mathcal{P}r_T(\mathbf{x})]. \quad (11)$$

Formulations of both kinds (i.e, the ones of (10) and of (11)) are widely used for solving medical physics problems and the question “Which of these two formulations leads to faster or better solutions of the underlying physical problem?” is open. Examples of both formulations with various choices for $\mathcal{P}r_T$ and ϕ are listed in the beginning parts of the paper of Goldstein and Osher⁴⁷.

We now return to the question raised near the end of Section I: Will superiorization produce superior results to those produced by contemporary MAP methods or is it faster than the better of such methods? As yet, there is very little information available regarding this general question; in fact, we are aware of only one published study⁴⁵. That study compared a superiorization algorithm with the algorithm of Goldstein and Osher that they refer to as TwIST⁴⁶ with split Bregman⁴⁷ as the substep, which is indeed a contemporary method that uses the MAP formulation. (For example, see the discussion of the split Bregman method in⁵⁶.) The problem S to which the two algorithms were applied was one from the tomographic problem set \mathbb{S} defined in (1). Res_S as defined in (2) was used as the proximity

function and total variation, TV as defined below in (12), was the choice for ϕ . It is reported in⁴⁵ that for the outputs of the two algorithms that were being compared, the values of Res_S and TV were very similar, but the superiorization algorithm produced its output four times faster than the MAP method.

III. AN ILLUSTRATIVE EXAMPLE

A. Application to tomography

We use *tomography* to refer to the process of reconstructing a function over a Euclidean space from estimated values of its integrals along lines (that are usually, but not necessarily, straight). The particular reconstruction processes to which our discussion applies are the *series expansion methods*, see Section 6.3 of⁵⁵, in which it is assumed that the function to be reconstructed can be approximated by a linear combination of a finite number (say J) of basis functions and the reconstruction task becomes one of estimating the coefficients of the basis functions in the expansion. Sometimes, prior knowledge about the nature of the function to be reconstructed allows us to confine the sought-after vector \mathbf{x} of coefficients to a subset Ω of \mathbb{R}^J (such as the nonnegative orthant \mathbb{R}_+^J). We use i to index the lines along which we integrate, $\mathbf{a}^i \in \mathbb{R}^J$ to denote the vector whose j th component is the integral of the j th basis function along the i th line, and b_i to denote the measured integral of the function to be reconstructed along the i th line. Under these circumstances the constraints come from the desire that, for each of the lines, $\langle \mathbf{a}^i, \mathbf{x} \rangle$ should be close (in some sense) to b_i .

To make this concrete, consider (1). Such a description of the constraints arises in tomography by grouping the lines of integration into W blocks, with ℓ_w lines in the w th block. Such groupings often (but not always) are done according to some geometrical condition on the lines (for example, in case of straight lines, we may decide that all the lines that are parallel to each other form one block). In this framework the proximity function Res defined by (2) provides a reasonable measure of the incompatibility of a vector \mathbf{x} with the constraints. The algorithm **R** described by (3) - (5) is applicable to this concrete formulation.

There are many optimization criteria that have been used in tomography, see Section 6.4 of⁵⁵, here we discuss the one called *total variation* (TV), whose use has been popular in medical physics recently, see as examples^{20,22,23,41-44}. The definition of TV that we use

here requires a certain way of selecting the basis functions. It is assumed that the function to be reconstructed is defined in the plane \mathbb{R}^2 and is zero-valued outside a square-shaped region in the plane. This region is subdivided into J smaller equal-sized squares (*pixels*) and the J basis functions are defined by having value one in exactly one pixel and value zero everywhere else. We index the pixels by j and we let C denote the set of all indices of pixels that are not in the rightmost column or the bottom row of the pixel array. For any pixel with index j in C , let $r(j)$ and $b(j)$ be the index of the pixel to its right and below it, respectively. We define $TV : \mathbb{R}^J \rightarrow \mathbb{R}$ by

$$TV(\mathbf{x}) = \sum_{j \in C} \sqrt{(x_j - x_{r(j)})^2 + (x_j - x_{b(j)})^2}. \quad (12)$$

The method we adopted to generate a nonascending vector for the TV function at an $\mathbf{x} \in \mathbb{R}^J$ is based on Theorem 2 of the Appendix. It is applicable since $TV : \mathbb{R}^J \rightarrow \mathbb{R}$ is a convex function; see, for example, the end of the Proof of Proposition 1 of⁴¹. Now consider an integer j' such that $1 \leq j' \leq J$. Looking at the sum in (12), we see that $x_{j'}$ appears in at most three terms, in which j' must be either j , or $r(j)$, or $b(j)$ for some $j \in C$. By taking the formal partial derivatives of these three terms, we see that $\frac{\partial TV}{\partial x_{j'}}(\mathbf{x})$ is well-defined if the denominator in the formal derivative of any of the three terms is not zero for \mathbf{x} . In view of this, we define the \mathbf{g} in Theorem 2 as follows. If the denominator in any of the three formal partial derivatives with respect to $x_{j'}$ has an absolute value less than a very small positive number (we used 10^{-20}), then we set $g_{j'}$ to zero, otherwise we set it to $\frac{\partial TV}{\partial x_{j'}}(\mathbf{x})$. Clearly the resulting $\mathbf{g} \in \mathbb{R}^J$ satisfies the condition in Theorem 2 and hence provides a \mathbf{d} that is a nonascending vector for TV at \mathbf{x} .

Previously reported reconstructions using TV -superiorization selected the \mathbf{d} using subgradients as discussed in the paragraph following (7); such a \mathbf{d} is not guaranteed to be a nonascending vector for the TV function. What we are proposing here is not only mathematically rigorous (in the sense that it is guaranteed to produce a nonascending vector for the TV function), but it can also lead to a better reconstructions, as illustrated in Subsection III D.

B. The data generation for the experiments

The data sets used in the experiments reported in this paper were generated in such a way that they share the noise-characteristics of CT scanners when used for scanning the human head and brain; as discussed, for example, in Chapter 5 of⁵⁵. They were generated using the software SNARK09⁵⁷.

The head phantom that was used for data generation is based on an actual cross-section of the human head. It is described as a collection of geometrical objects (such as ellipses, triangles and segments of circles) whose combination accurately resembles the anatomical features of the actual head cross-section. In addition, the basic phantom contains a large tumor. The actual phantom used was obtained by a random variation of the basic phantom, by incorporating into it local inhomogeneities and small low-contrast tumors at random locations. This phantom is represented by the image in figure 1. That image comprises 485×485 pixels each of size 0.376 mm by 0.376 mm. The values assigned to the pixels are obtained by an 11×11 sub-sampling of the pixels and averaging the values assigned to the sub-samples by the geometrical objects that are used to describe the anatomical features and the tumors. Those values are approximate linear attenuation coefficients per cm at 60 keV (0.416 for bone, 0.210 for brain, 0.207 for cerebrospinal fluid). The contrast of the small tumors with their background is 0.003 cm^{-1} . In order to clearly see the low-contrast details in the interior of the skull, we use zero (black) to represent the value 0.204 (or anything less) and 255 (white) to represent 0.21675 or anything more).

For the selected head phantom we generated *parallel projection data*, in which one *view* comprises estimates of integrals through the phantom for a set of 693 equally-spaced parallel lines with a spacing of 0.0376 cm between them. (We chose to simulate parallel rather than divergent projection data, since the reconstruction by the method of⁴² with which we wish to compare the superiorization approach were performed for us by the authors of⁴² on parallel data. Even though contemporary CT scanners use divergent projection data, results obtained by the use of parallel projection data are relevant to them, since it is known that the quality of reconstructions from these two modes of data collection are very similar as long as the data generations use similar frequencies of sampling of lines and similar noise characteristics in the estimated integrals for those lines; see, for example, the reconstructions from divergent and parallel projection data in figure 5.15 of⁵⁵.) In calculating

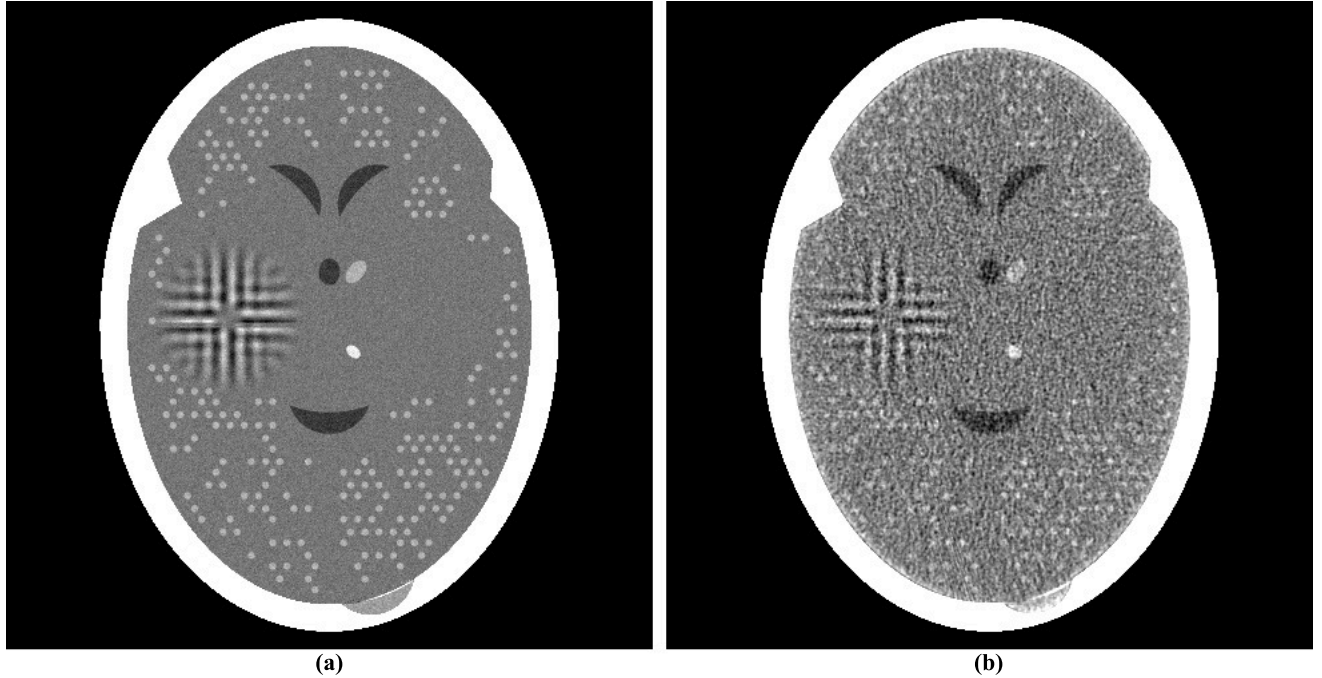


Figure 1: (a) A head phantom. (b) Reconstruction of the head phantom from realistically simulated projection data for 360 views using ART with blob basis functions.

573 these estimates we take into consideration the effects of photon statistics, detector width
 574 and scatter. Details of how we do this exactly can be found in Sections 5.5 and 5.9 of⁵⁵.
 575 Briefly, quantum noise is calculated based on the assumption that approximately 2,000,000
 576 photons enter the head along each ray, detector width is simulated by using 11 sub-rays
 577 along each of which the attenuation is calculated independently and then combined at the
 578 detector, and 5% of the photons get counted not by the detector for the ray in question but
 579 detectors for the neighboring rays. For the experiments in this paper, we did not simulate
 580 the poly-energetic nature of the x-ray source. To indicate what can be achieved in clinical
 581 CT, we show in figure 1(b) a reconstruction that was made from data comprising of 360
 582 such views with the reconstruction algorithm known as ART with blob basis functions; see⁵⁵
 583 (Chapter 11).

584 C. Superiorization reconstruction from a few views

585 The main reason in the literature for advocating the use of TV as the optimization
 586 criterion is that by doing so one can achieve efficacious reconstructions even from sparsely

sampled data. In our own work³¹ with realistically simulated CT data we found that this is not always the case and this will be demonstrated again by the experiments reported in the current paper.

There have appeared in the literature some approaches to TV minimization that seem to indicate a more efficacious performance for CT than the one reported in³¹. One of these is the Adaptive Steepest Descent Projections Onto Convex Sets (ASD-POCS) algorithm, which is described in detail in the much-cited paper of Sidky and Pan⁴² and whose use has been since reported in a number of subsequent publications, for example, in^{23,43}. We note that ASD-POCS was designed with the aim of producing an exact minimization algorithm, in contrast to our heuristic superiorization approach. Translating equations (6)-(8) of⁴² into our terminology, the aim of ASD-POCS is the following: Given an $\varepsilon \in \mathbb{R}_+$, find an ε -compatible $\mathbf{x} \in \Omega = \mathbb{R}_+^J$ for which $TV(\mathbf{x})$ is minimal. (Note that this aim is a special case of the constrained optimization formulation presented in (10).) In order to test ASD-POCS, we generated realistic projection data as described in the previous subsection but for only 60 views at 3 degree increments with the spacing between the lines for which integrals are estimated set at 0.752 mm. Thus the number of rays (and hence the number photons put into the head) in this data set is a twelfth of what it is in the data set used to produce the reconstruction in figure 1(b). A reconstruction from these data was produced for us using ASD-POCS by the authors of⁴² (this ensured that it does not suffer due to our misinterpretation of the algorithm or from our inappropriate choices of the free parameters), it is shown in figure 2(a).

Since the image quality of figure 2(a) is not anywhere near to that of figure 1(b), we present here a brief discussion as to why we are showing such images. Many publications in the recent medical imaging literature have claimed that medically-efficacious reconstructions can be obtained by the use of TV -minimization from data as sparse as what was used to produce figure 2(a). (In fact, ASD-POCS was motivated and used with such an aim in mind^{23,42,43}.) Such publications usually show reconstructions from sparse data as evidence for the validity of their claims. They can do this because in their presented illustrations the features that are observable in the reconstructions are usually much larger and/or of much higher contrast against their backgrounds than the small “tumors” in figure 1(a), which are perfectly visible in the reconstruction in figure 1(b), but are not detectable in the reconstruction from sparse data in figure 2(a). The reason why that reconstruction appears to be unacceptably bad is

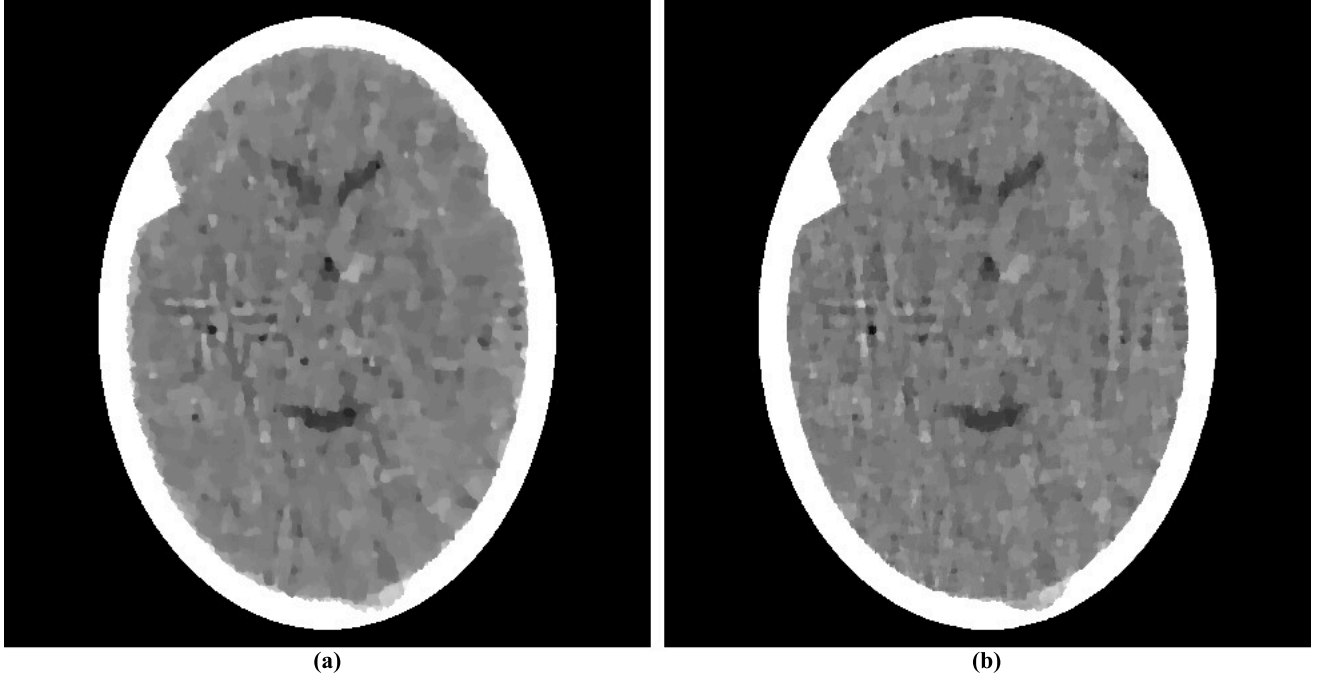


Figure 2: Reconstructions using TV as the optimization criterion from realistically simulated projection data for 60 views using (a) ASD-POCS and (b) superiorization. As compared to figure 1(b), these reconstructions fail in two ways: they do not show some of the fine details in the phantom and they present some artifactual variations. The former of these is a consequence of reconstructing from a much smaller data set than used for figure 1(b). The latter is due to using a very narrow window (13.5 HU) in these displays. Were we to use a wider display window (e.g., from -429 HU to 429 HU) for the reconstructions in this figure and in figure 1(b), the visual appearance of the resulting images would be nearly indistinguishable.

619 that the display window (from 0.204 cm^{-1} linear attenuation coefficient to 0.21675 cm^{-1} linear
620 attenuation coefficient) is very narrow; it was selected to enhance the visibility of the small
621 low-contrast tumors. The width of this window corresponds to about 13.5 Hounsfield Units
622 (HU). As compared to this, in their evaluation of sparse-view reconstruction from flat-panel-
623 detector cone-beam CT, Bian *et al.*⁴³ use what they call a “soft-tissue grayscale window”
624 (also a “narrow window”) from -429 HU to 429 HU to display head phantom reconstructions.
625 Using such a window for our reconstructions shown figures 2(a) and 1(b) would result in
626 images that are nearly indistinguishable from each other. Thus reporting the images using
627 such a display window is consistent with the claim that a TV-minimizing reconstruction

from a few views is similar in quality to a more traditional reconstruction from many views. However, our much narrower display window reveals that this is not really so. We therefore continue using our much narrower window in what follows, since it clearly reveals the nature of the reconstructions being compared, warts and all.

While this ASD-POCS reconstruction is not as good as it should be for diagnostic CT of the brain (due to the sparsity of the data), it is visually better than the reconstruction using superiorization from similar data as reported in³¹. We discuss the reasons for this in the next subsection. Here we concentrate on examining whether one can achieve a reconstruction using superiorization that is as good as that produced by ASD-POCS from the same data.

For this we first need to examine the numerical properties of the ASD-POCS reconstruction. This reconstruction uses 485×485 pixels each of size 0.376 mm by 0.376 mm. This implies that $J = 235,225$ and it also determines the components of the vectors $\mathbf{a}^i \in \mathbb{R}^J$ in the precise specification of the problem S . The Res_S , as defined by (2), of the ASD-POCS reconstruction is 0.33 and the TV , as defined by (12), is 835.

We applied to the same problem S a superiorized version of the algorithm \mathbf{R} defined by (3). To complete the specification of \mathbf{R} , we point out that for the ordering of views we chose the “efficient” one that was introduced in⁵⁸ and is also discussed on page 209 of⁵⁵. The choices we made for the superiorization are the following: $\gamma_\ell = 0.99995^\ell$, $\bar{\mathbf{x}}$ is the zero vector and $N = 20$. The nonascending vector was computed by the method described in the paragraph below (12). Denoting by R_S the infinite sequence of points in Ω that is produced by the superiorized version of the algorithm \mathbf{R} when applied to the problem S , we chose as our reconstruction $\mathbf{x}^* = O(S, 0.33, R_S)$. For such a reconstruction we have, by the definition of O , that $Res_S(\mathbf{x}^*) \leq 0.33$; in other words, the output of the superiorization algorithm is at least as constraints-compatible with S as the output of ASD-POCS. From the point of view of TV -minimization, our \mathbf{x}^* is slightly better: $TV(\mathbf{x}^*) = 826$.

The superiorization reconstruction is displayed in figure 2(b). Visually it is similar to the reconstruction produced by ASD-POCS. From the optimization point of view it achieves the desired aim better than ASD-POCS does, since it results in smaller values for both Res_S and for TV , even though only slightly.

That the two reconstructions in figure 2 are very similar is not surprising because a comparison of the pseudo-codes reveals that the ASD-POCS algorithm in⁴² is essentially a special case of the Superiorized Version of Algorithm \mathbf{P} , even though it has been derived

660 from rather different principles. To obtain the ASD-POCS algorithm from our methodology
 661 described here, we would have to choose an Algebraic Reconstruction Technique (ART;
 662 see Chapter 11 of⁵⁵) as the algorithm that we are superiorizing. Such a superiorization of
 663 ART was reported in the earliest paper on superiorization²⁷. For the illustration in our
 664 current paper we decided to superiorize the block-iterative algorithm \mathbf{R} defined by (3).
 665 This illustrates the generality of the superiorization approach: it is applicable not only to
 666 a large class of constrained optimization problems, but also enables the use of any of a
 667 large class of iterative algorithms designed to produce a constraints-compatible solutions.
 668 A recent publication aimed at producing an exact TV -minimizing algorithm based on the
 669 block-iterative approach is⁴⁴.

670 D. Effects of variations in the reconstruction approach

671 The reconstruction in figure 2(a) produced by ASD-POCS definitely “looks better” than
 672 a reconstruction in³¹, which was obtained using superiorization from similar data. Since, as
 673 discussed in the last paragraph of the previous subsection, the ASD-POCS algorithm in⁴²
 674 can be obtained as a special case of superiorization, it must be that some of the choices made
 675 in the details of the implementations are responsible for the visual differences. An analysis
 676 of the implementational details adopted by the two approaches revealed several differences.
 677 After removing these differences, the superiorization approach produced the image in figure
 678 2(b), which is very similar to the reconstruction produced by ASD-POCS. We now list the
 679 implementational choices that were made for superiorization to make its performance match
 680 that of the reported implementation of ASD-POCS.

681 One implementational difference is in the stopping-rule of the iterative algorithm; that
 682 is, the choice of ε in determining the output $O(S, \varepsilon, R_S)$. Since the data are noisy, the
 683 phantom itself does not match the data exactly. In previously reported implementations of
 684 superiorization it was assumed that the iterative process should terminate when an image
 685 is obtained that is approximately as constraints-compatible as the phantom; in the case of
 686 the phantom and the projections data on which we report here the value of Res_S for the
 687 phantom is approximately 0.91, which is larger than its value (0.33) for the reconstruction
 688 produced by ASD-POCS. The output $O(S, 0.91, R_S)$ is shown in figure 3(a). This is a
 689 wonderfully smooth reconstruction, its TV value is only 771. However this smoothness

comes at a price: we loose not only the ability to detect the large tumor, but we cannot even see anatomic features (such as the ventricular cavities) inside the brain. So it appears that, in order to see medically-relevant features in the brain, *over-fitting* (in the sense of producing a reconstruction from noisy data that is more constraints-compatible than the phantom) is desirable.

In the implementations that produced previously reported reconstructions by superiorization, the number N in the Superiorized Version of Algorithm **P** was always chosen to be 1. It is possible that this is the wrong choice, making only this change to what lead to the reconstruction in figure 2(b) results in the reconstruction shown in figure 3(b). That image appears similar to the image in figure 2(b), but it has a higher TV value, namely 832, which is still very slightly lower than that of the ASD-POCS reconstruction. The choice $N = 20$ was based on the desire to maintain consistency with what has been practiced using ASD-POCS, see page 4790 of⁴². It appears that in the context of our paper the additional computing cost due to choosing N to be 20 rather than 1 is not really justified. (We note that if \mathbf{d} is selected using subgradients as discussed in the paragraph following (7) and thus \mathbf{d} is not guaranteed to be a nonascending vector for the TV function, then the choice of 20 rather than 1 for N results in a considerable improvement. However, an even greater improvement is achieved even with $N = 1$ by selecting \mathbf{d} as recommended in this paper.)

Another important difference between the ASD-POCS implementation and the previous implementations of the superiorization approach is the size of the pixels in the reconstructions. For the ASD-POCS reconstruction this was selected to be 0.376 mm by 0.376 mm. In previously reported reconstructions by superiorization it was assumed that the edge of a pixel should be the same as the distance between the parallel lines along which the data are collected; that is, 0.752 mm for our problem S . This assumption proved to be false. TV -minimization takes care of undesirable artifacts that may otherwise arise due to the smaller pixels and this leads to a visual improvement. A superiorizing reconstruction with the larger pixels, using $\varepsilon = 0.33$ and $N = 20$, is shown in figure 3(c). (We note that the use of smaller pixels during iterative x-ray CT reconstructions was also suggested in⁵⁹. However, that approach is quite different from what is presented here: its final result uses larger pixels whose values are obtained by averaging assemblies of values provided by the iterative process to the smaller pixels. There is no such downsampling in our approach, our final result is presented using the smaller pixels. Its smoothness is due to reduction of TV by the

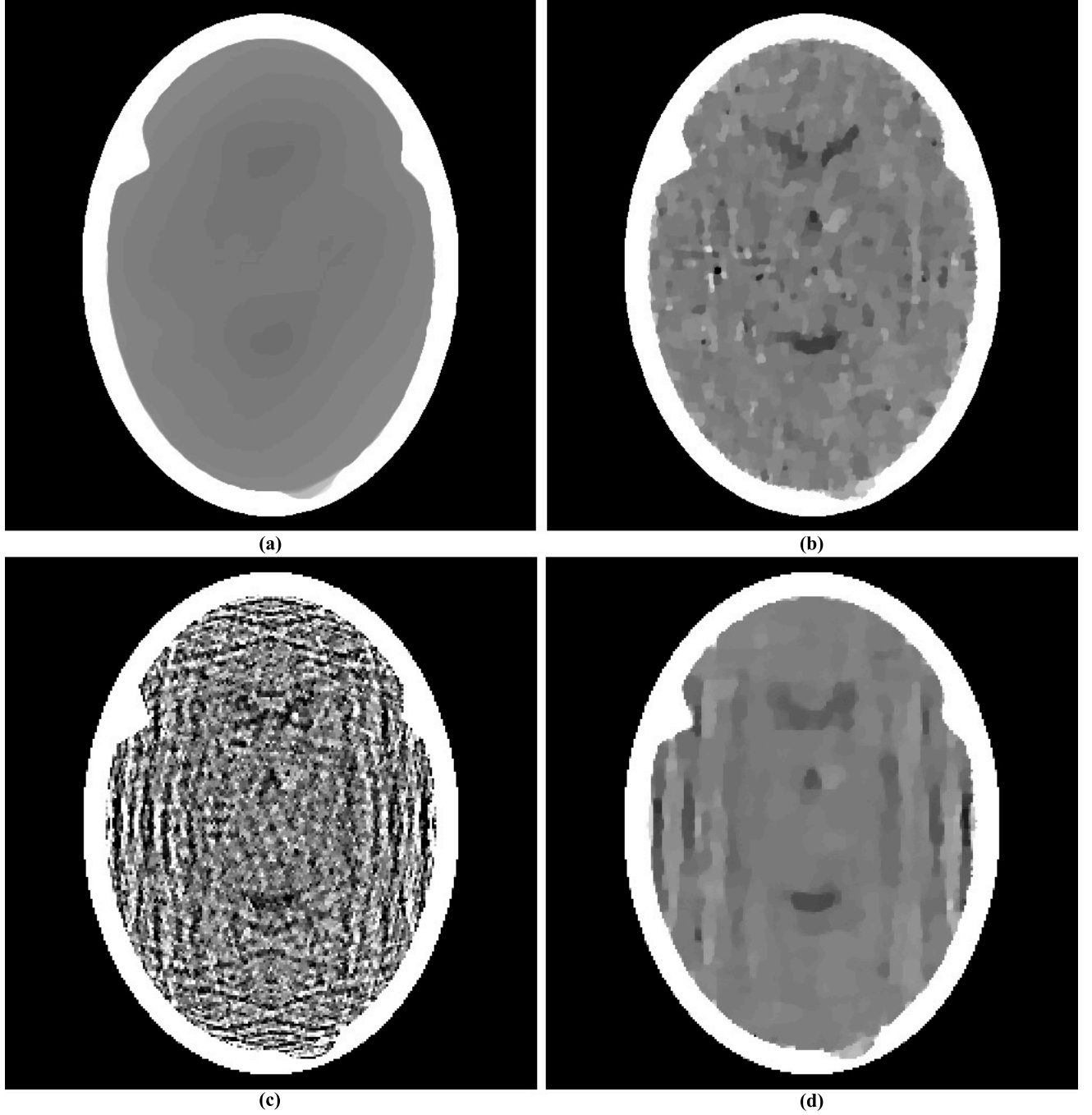


Figure 3: Reconstructions produced by varying some of the parameters in the algorithm that produced figure 2(b). (a) Changing the termination criterion from $\varepsilon = 0.33$ to $\varepsilon = 0.91$. (b) Changing the value of N from 20 to 1. (c) Reconstructing with pixel size 0.752 mm by 0.752 mm instead of 0.376 mm by 0.376 mm. (d) Reconstructing with all the three changes of (a)-(c).

superiorization approach rather than to averaging pixel values in a denser digitization.)

Combining the use of the larger pixels with $\varepsilon = 0.91$ and $N = 1$ results in the reconstruction shown in figure 3(d). This reconstruction, for which the superiorization options were selected according to what was done in³¹, is visually inferior to those shown in our figure 2. The reconstructions displayed in figure 3 also illustrate another important point, namely that even though the mathematical results discussed in this paper are valid for a large range of choices of the parameters in the superiorization algorithms, for medical efficacy of the reconstructions attention has to be paid to these choices since they can have a drastic effect on the quality of the reconstruction.

It has been mentioned in Subsection IIB that except for the presence of \mathbf{Q} in (3), which enforces nonnegativity of the components, \mathbf{R} is identical to the algorithm used and illustrated in³¹. It is known that CT reconstruction of the brain from many views does not suffer from ignoring the fact that the components of the \mathbf{x} , which represent linear attenuation coefficients, should be nonnegative; as is illustrated in figure 1(b). This remains so when reconstructing from a few views using the method and data that we have been discussing: if we do everything in exactly the same way as was done to obtain the reconstruction with TV value 826 that is shown in our figure 2(b) but remove \mathbf{Q} from (3), then we obtain a reconstruction in figure 4(a) whose TV value is 829.

Another variation that deserves discussion, because it has been suggested in the literature²², is one that does not come about by making choices for the general approach of the Superiorized Version of Algorithm \mathbf{P} but rather by changing the nature of the approach. The variation in question is not applicable in general, but can be applied to the special case when the algorithm to be superiorized is the \mathbf{R} defined by (3). It was suggested as an improvement to the approach presented above with the choice $N = 1$. The idea was based on recognizing the block-iterative nature of the algorithmic operator \mathbf{R}_S in (3) and intermingling the perturbation steps of lines (vii)-(xvii) of the Superiorized Version of Algorithm \mathbf{R} with the projection steps $\mathbf{B}_{S_1}, \dots, \mathbf{B}_{S_W}$ of (3). It was reported in²² that doing this is advantageous to using the Superiorized Version of Algorithm \mathbf{R} . However, when we applied the variation of the Superiorized Version of Algorithm \mathbf{R} that is proposed in²² to the problem S that we have been using in this section, we ended up with the reconstruction in figure 4(b) whose TV value is 920. This is not as good as what was obtained using the version of the algorithm that produced the reconstruction in figure 2(b). We conclude that

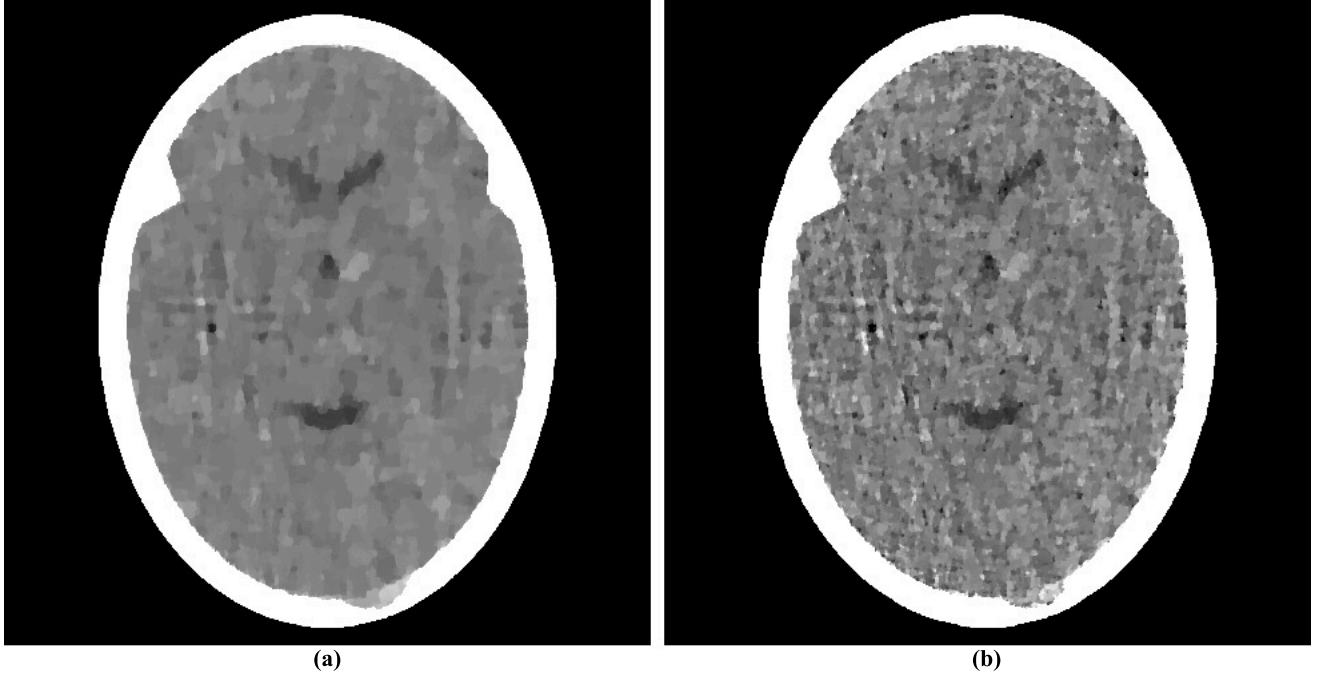


Figure 4: Reconstructions by variations that do not fit into the framework within which the previously shown reconstructions were produced. (a) Not using nonnegativity in the algorithm. (b) Interleaving perturbations with blocks.

the variation suggested by²², which does not fit into the theory of our paper, does not have an advantage over what we are proposing here, at least for the problem S that we have been discussing in this section. We conjecture that the improvement reported in²² is due to selecting \mathbf{d} using subgradients as discussed in the paragraph following (7) and, as discussed earlier, such an improvement is not obtained if \mathbf{d} is selected by the more appropriate method recommended in this paper.

IV. DISCUSSION AND CONCLUSIONS

Constrained optimization is an often-used tool in medical physics. The methodology of superiorization is a heuristic (as opposed to exact) approach to constrained optimization.

Although the idea of superiorization was introduced in 2007 and its practical use has been demonstrated in several publications since, this paper is the first to provide a solid mathematical foundation to superiorization as applied to the noisy problems of the real world. These foundations include a precise definition of constraints-compatibility, the concept of a

strongly perturbation resilient algorithm, simple conditions that ensure that an algorithm is strongly perturbation resilient, the superiorized version of an algorithm and the showing that the superiorized version of a strongly perturbation resilient algorithm produces outputs that are essentially as constraints-compatible as those produced by the original version but are likely to have a smaller value of the chosen optimization criterion.

The approach is very general. For any iterative algorithm \mathbf{P} and for any optimization criterion ϕ for which we know how to produce nonascending vectors, the pseudocode given in Subsection IIE automatically provides the version of \mathbf{P} that is superiorized for ϕ .

We demonstrated superiorization for tomography when total variation is used as the optimization criterion. In particular, we illustrated on a particular tomography problem that, in spite of its generality, superiorization produced a reconstruction that is as good as (from the points of view of constraints-compatibility and TV -minimization) what was obtained by the ASD-POCS algorithm that was specially designed for TV -minimization in tomography.

Acknowledgments

The detailed and penetrating comments of three reviewers and the editors helped us to improve this paper in a significant way. We thank Prof. Xiaochuan Pan and his coworkers from the University of Chicago for providing us with the reconstruction from our data using their implementation of their ASD-POCS algorithm. Our work is supported by the National Science Foundation award number DMS-1114901, the United States-Israel Binational Science Foundation (BSF) grant number 200912, and the US Department of Army award number W81XWH-10-1-0170.

Appendix

Conditions for strong perturbation resilience

Theorem 1. Let \mathbf{P} be an algorithm for a problem structure $\langle \mathbb{T}, \mathcal{P}r \rangle$ such that, for all $T \in \mathbb{T}$, \mathbf{P} is boundedly convergent for T , $\mathcal{P}r_T : \Omega \rightarrow \mathbb{R}$ is uniformly continuous and $\mathbf{P}_T : \Delta \rightarrow \Omega$ is nonexpansive. Then \mathbf{P} is strongly perturbation resilient.

794 *Proof.* We first show that there exists an $\varepsilon \in \mathbb{R}_+$ such that $O\left(T, \varepsilon, \left((\mathbf{P}_T)^k \mathbf{x}\right)_{k=0}^\infty\right)$
 795 is defined for every $\mathbf{x} \in \Omega$. Under the assumptions of the theorem, let $\gamma \in \mathbb{R}_+$ be such
 796 that $\mathcal{P}r_T(\mathbf{y}(\mathbf{x})) \leq \gamma$, for every $\mathbf{x} \in \Omega$. We prove that $O\left(T, 2\gamma, \left((\mathbf{P}_T)^k \mathbf{x}\right)_{k=0}^\infty\right)$ is defined
 797 for every $\mathbf{x} \in \Omega$ as follows. Select a particular $\mathbf{x} \in \Omega$. By uniform continuity of $\mathcal{P}r_T$,
 798 there exists a $\delta > 0$, such that $|\mathcal{P}r_T(\mathbf{z}) - \mathcal{P}r_T(\mathbf{y}(\mathbf{x}))| \leq \gamma$, for any $\mathbf{z} \in \Omega$ for which
 799 $\|\mathbf{z} - \mathbf{y}(\mathbf{x})\| \leq \delta$. Since \mathbf{P} is convergent for T , there exists a nonnegative integer K , such
 800 that $\left\|(\mathbf{P}_T)^K \mathbf{x} - \mathbf{y}(\mathbf{x})\right\| \leq \delta$. It follows that

$$\begin{aligned} \left|\mathcal{P}r_T\left((\mathbf{P}_T)^K \mathbf{x}\right)\right| &\leq \left|\mathcal{P}r_T\left((\mathbf{P}_T)^K \mathbf{x}\right) - \mathcal{P}r_T(\mathbf{y}(\mathbf{x}))\right| + |\mathcal{P}r_T(\mathbf{y}(\mathbf{x}))| \\ &\leq 2\gamma. \end{aligned} \quad (13)$$

801 Now let $T \in \mathbb{T}$ and $\varepsilon \in \mathbb{R}_+$ be such that $O\left(T, \varepsilon, \left((\mathbf{P}_T)^k \mathbf{x}\right)_{k=0}^\infty\right)$ is defined for every
 802 $\mathbf{x} \in \Omega$. To prove the theorem, we need to show that $O\left(T, \varepsilon', R\right)$ is defined for every $\varepsilon' > \varepsilon$
 803 and for every sequence $R = (\mathbf{x}^k)_{k=0}^\infty$ of points in Ω for which, for all $k \geq 0$, (6) is satisfied for
 804 bounded perturbations $\beta_k \mathbf{v}^k$. Let ε' and R satisfy the conditions of the previous sentence.

For $k \geq 0$, we have, due to the nonexpansiveness of \mathbf{P}_T , that

$$\|\mathbf{x}^{k+1} - \mathbf{P}_T \mathbf{x}^k\| = \|\mathbf{P}_T(\mathbf{x}^k + \beta_k \mathbf{v}^k) - \mathbf{P}_T \mathbf{x}^k\| \leq \|\beta_k \mathbf{v}^k\|. \quad (14)$$

805 Denote $\|\beta_k \mathbf{v}^k\|$ by r_k . Clearly, $r_k \in \mathbb{R}_+$ and it follows from the definition of bounded
 806 perturbations that $\sum_{k=0}^\infty r_k < \infty$.

807 We next prove by induction that, for every pair of nonnegative integers k and i ,

$$\left\|\mathbf{x}^{k+i} - (\mathbf{P}_T)^i \mathbf{x}^k\right\| \leq \sum_{j=k}^{k+i-1} r_j. \quad (15)$$

808 Let k be an arbitrary nonnegative integer. If $i = 0$, then the value is zero on both sides of
 809 the inequality and hence (15) holds. Now assume that (15) holds for an integer $i \geq 0$. Then,
 810 by (14) and the nonexpansiveness of \mathbf{P}_T ,

$$\begin{aligned} \left\|\mathbf{x}^{k+i+1} - (\mathbf{P}_T)^{i+1} \mathbf{x}^k\right\| &\leq \left\|\mathbf{x}^{k+i+1} - \mathbf{P}_T \mathbf{x}^{k+i}\right\| \\ &\quad + \left\|\mathbf{P}_T \mathbf{x}^{k+i} - (\mathbf{P}_T)^{i+1} \mathbf{x}^k\right\| \\ &\leq r_{k+i} + \left\|\mathbf{x}^{k+i} - (\mathbf{P}_T)^i \mathbf{x}^k\right\| \\ &\leq r_{k+i} + \sum_{j=k}^{k+i-1} r_j \\ &= \sum_{j=k}^{k+i} r_j, \end{aligned} \quad (16)$$

which completes our inductive proof. A consequence of (15) is that, for every pair of non-negative integers k and i ,

$$\left\| \mathbf{x}^{k+i} - (\mathbf{P}_T)^i \mathbf{x}^k \right\| \leq \sum_{j=k}^{\infty} r_j. \quad (17)$$

Due to the summability of the nonnegative sequence $(r_k)_{k=0}^{\infty}$, the right-hand side (and hence the left-hand side) of this inequality gets arbitrarily close to zero as k increases.

Since $\mathcal{P}r_T$ is uniformly continuous, there exists a δ such that, for all $\mathbf{x}, \mathbf{y} \in \Omega$, $|\mathcal{P}r_T(\mathbf{x}) - \mathcal{P}r_T(\mathbf{y})| \leq \varepsilon' - \varepsilon$ provided that $\|\mathbf{x} - \mathbf{y}\| \leq \delta$. Select a k so that $\sum_{j=k}^{\infty} r_j \leq \delta$. By the assumption that $O\left(T, \varepsilon, \left((\mathbf{P}_T)^k \mathbf{x}\right)_{k=0}^{\infty}\right)$ is defined for every $\mathbf{x} \in \Omega$, there exists a nonnegative integer i for which $\mathcal{P}r\left((\mathbf{P}_T)^i \mathbf{x}^k\right) \leq \varepsilon$. From (17) we have, for this k and i , that $\left\| \mathbf{x}^{k+i} - (\mathbf{P}_T)^i \mathbf{x}^k \right\| \leq \delta$ and, hence,

$$\begin{aligned} |\mathcal{P}r_T(\mathbf{x}^{k+i})| &\leq \left| \mathcal{P}r_T(\mathbf{x}^{k+i}) - \mathcal{P}r_T\left((\mathbf{P}_T)^i \mathbf{x}^k\right) \right| \\ &\quad + \left| \mathcal{P}r_T\left((\mathbf{P}_T)^i \mathbf{x}^k\right) \right| \\ &\leq (\varepsilon' - \varepsilon) + \varepsilon = \varepsilon', \end{aligned} \quad (18)$$

proving that $O(T, \varepsilon', R)$ is defined. \square

Nonascending vectors for convex functions

Theorem 2. Let $\phi : \mathbb{R}^J \rightarrow \mathbb{R}$ be a convex function and let $\mathbf{x} \in \mathbb{R}^J$. Let $\mathbf{g} \in \mathbb{R}^J$ satisfy the property: For $1 \leq j \leq J$, if the j th component g_j of \mathbf{g} is not zero, then the partial derivative $\frac{\partial \phi}{\partial x_j}(\mathbf{x})$ of ϕ at \mathbf{x} exists and its value is g_j . Define \mathbf{d} to be the zero vector if $\|\mathbf{g}\| = 0$ and to be $-\mathbf{g}/\|\mathbf{g}\|$ otherwise. Then \mathbf{d} is a nonascending vector for ϕ at \mathbf{x} .

Proof. The theorem is trivially true if $\|\mathbf{g}\| = 0$, so we assume that this is not the case. We denote by I the nonempty set of those indices j for which $g_j \neq 0$.

For $1 \leq j \leq J$, let s_j be $g_j/|g_j|$ for $j \in I$ and be 0 otherwise, and let $\mathbf{e}^j \in \mathbb{R}^J$ be the vector all of whose components are zero except for the j th, which is one. Then, for $1 \leq j \leq J$, there exists a $\delta_j > 0$ such that, for $0 \leq \lambda_j \leq \delta_j$,

$$\phi(\mathbf{x} - \lambda_j s_j \mathbf{e}^j) \leq \phi(\mathbf{x}). \quad (19)$$

This is obvious if $s_j = 0$. Otherwise, $\frac{\partial \phi}{\partial x_j}(\mathbf{x})$ exists and indicates ϕ increases at \mathbf{x} if $s_j = 1$ or that ϕ decreases at \mathbf{x} if $s_j = -1$. The existence of the desired δ_j can be derived from the standard definition of the partial derivative as a limit.

834 We define $\delta > 0$ by

$$\delta = \frac{\|\mathbf{g}\|}{J} \min_{j \in I} \left\{ \frac{\delta_j}{|g_j|} \right\}. \quad (20)$$

835 Then we have that, for $0 \leq \lambda \leq \delta$,

$$\begin{aligned} \phi(\mathbf{x} + \lambda \mathbf{d}) &= \phi \left(\mathbf{x} - \lambda \sum_{j=1}^J \frac{|g_j|}{\|\mathbf{g}\|} s_j \mathbf{e}^j \right) \\ &= \phi \left(\sum_{j=1}^J \frac{1}{J} \left(\mathbf{x} - \lambda J \frac{|g_j|}{\|\mathbf{g}\|} s_j \mathbf{e}^j \right) \right) \\ &\leq \frac{1}{J} \sum_{j=1}^J \phi \left(\mathbf{x} - \lambda J \frac{|g_j|}{\|\mathbf{g}\|} s_j \mathbf{e}^j \right) \\ &\leq \frac{1}{J} \sum_{j=1}^J \phi(\mathbf{x}) \\ &= \phi(\mathbf{x}). \end{aligned} \quad (21)$$

836 The first inequality above follows from the convexity of ϕ and the second one follows from
 837 (19), with λ_j defined to be $\lambda J \frac{|g_j|}{\|\mathbf{g}\|}$, combined with (20). Thus \mathbf{d} is a nonascending vector for
 838 ϕ at \mathbf{x} . \square

839 * Author to whom correspondence should be addressed; Electronic address: [gaborther-](mailto:gabortherman@yahoo.com)
 840 man@yahoo.com; URL: <http://www.dig.cs.gc.cuny.edu/~gabor/index.html>

841 ¹ J. O. Deasy, "Multiple local minima in radiotherapy optimization problems with dose-volume
 842 constraints," *Med. Phys.* **24**, 1157–1161, (1997).

843 ² G. A. Ezzell, "Genetic and geometric optimization of three-dimensional radiation therapy treat-
 844 ment planning," *Med. Phys.* **23**, 293–305, (1996).

845 ³ A. Gustafsson, B. K. Lind, and A. Brahme, "A generalized pencil beam algorithm for optimiza-
 846 tion of radiation-therapy," *Med. Phys.* **21**, 343–357, (1994).

847 ⁴ A. Gustafsson, B. K. Lind, R. Svensson, and A. Brahme, "Simultaneous-optimization of dynamic
 848 multileaf collimation and scanning patterns or compensation filters using a generalized pencil
 849 beam algorithm," *Med. Phys.* **22**, 1141–1156, (1995).

850 ⁵ E. Lessard and J. Pouliot, "Inverse planning anatomy-based dose optimization for hdr-
 851 brachytherapy of the prostate using fast simulated annealing algorithm and dedicated objective
 852 function," *Med. Phys.* **28**, 773–779, (2001).

- 853 ⁶ R. Manzke, M. Grass, T. Nielsen, G. Shechter, and D. Hawkes, "Adaptive temporal resolution
854 optimization in helical cardiac cone beam CT reconstruction," *Med. Phys.* **30**, 3072–3080, (2003).
- 855 ⁷ A. B. Pugachev, A. L. Boyer, and L. Xing, "Beam orientation optimization in intensity-
856 modulated radiation treatment planning," *Med. Phys.* **27**, 1238–1245, (2000).
- 857 ⁸ D. M. Shepard, M. A. Earl, X. A. Li, S. Naqvi, and C. Yu, "Direct aperture optimization: A
858 turnkey solution for step-and-shoot IMRT," *Med. Phys.* **29**, 1007–1018, (2002).
- 859 ⁹ C. Studholme, D. L. G. Hill, and D. J. Hawkes, "Automated three-dimensional registration of
860 magnetic resonance and positron emission tomography brain images by multiresolution opti-
861 mization of voxel similarity measures," *Med. Phys.* **24**, 25–35, (1997).
- 862 ¹⁰ Q. W. Wu and R. Mohan, "Algorithms and functionality of an intensity modulated radiotherapy
863 optimization system," *Med. Phys.* **27**, 701–711, (2000).
- 864 ¹¹ Y. Yu and M. C. Schell, "A genetic algorithm for the optimization of prostate implants," *Med.*
865 *Phys.* **23**, 2085–2091, (1996).
- 866 ¹² T. Z. Zhang, R. Jeraj, H. Keller, W. G. Lu, G. H. Olivera, T. R. McNutt, T. R. Mackie, and
867 B. Paliwal, "Treatment plan optimization incorporating respiratory motion," *Med. Phys.* **31**,
868 1576–1586, (2004).
- 869 ¹³ M. Abdoli, M. R. Ay, A. Ahmadian, R. A. Dierckx, and H. Zaidi, "Reduction of dental fill-
870 ing metallic artifacts in CT-based attenuation correction of PET data using weighted virtual
871 sinograms optimized by a genetic algorithm," *Med. Phys.* **37**, 6166–6177, (2010).
- 872 ¹⁴ S. Bartolac, S. Graham, J. Siewerdsen, and D. Jaffray, "Fluence field optimization for noise and
873 dose objectives in CT," *Med. Phys.* **38**, S2–S17, (2011).
- 874 ¹⁵ W. Chen, D. Craft, T. M. Madden, K. Zhang, H. M. Kooy, and G. T. Herman, "A fast opti-
875 mization algorithm for multicriteria intensity modulated proton therapy planning," *Med. Phys.*
876 **37**, 4938–4945, (2010).
- 877 ¹⁶ J. Fiege, B. McCurdy, P. Potrebko, H. Champion, and A. Cull, "PARETO: A novel evolutionary
878 optimization approach to multiobjective IMRT planning," *Med. Phys.* **38**, 5217–5229, (2011).
- 879 ¹⁷ A. Fredriksson, A. Forsgren, and B. Hardemark, "Minimax optimization for handling range and
880 setup uncertainties in proton therapy," *Med. Phys.* **38**, 1672–1684, (2011).
- 881 ¹⁸ C. Holdsworth, M. Kim, J. Liao, and M. H. Phillips, "A hierarchical evolutionary algorithm for
882 multiobjective optimization in IMRT," *Med. Phys.* **37**, 4986–4997, (2010).
- 883 ¹⁹ C. Holdsworth, R. D. Stewart, M. Kim, J. Liao, and M. H. Phillips, "Investigation of effective

- 884 decision criteria for multiobjective optimization in IMRT,” *Med. Phys.* **38**, 2964–2974, (2011).
- 885 ²⁰ T. Kim, L. Zhu, T.-S. Suh, S. Geneser, B. Meng, and L. Xing, “Inverse planning for IMRT with
886 nonuniform beam profiles using total-variation regularization (TVR),” *Med. Phys.* **38**, 57–66,
887 (2011).
- 888 ²¹ C. Men, H. E. Romeijn, X. Jia, and S. B. Jiang, “Ultrafast treatment plan optimization for
889 volumetric modulated arc therapy (VMAT),” *Med. Phys.* **37**, 5787–5791, (2010).
- 890 ²² S. N. Penfold, R. W. Schulte, Y. Censor, and A. B. Rosenfeld, “Total variation superiorization
891 schemes in proton computed tomography image reconstruction,” *Med. Phys.* **37**, 5887–5895,
892 (2010).
- 893 ²³ E. Y. Sidky, Y. Duchin, X. Pan, and C. Ullberg, “A constrained, total-variation minimization
894 algorithm for low-intensity x-ray CT,” *Med. Phys.* **38**, S117–S125, (2011).
- 895 ²⁴ H. Stabenau, L. Rivera, E. Yorke, J. Yang, R. Lu, R. J. Radke, and A. Jackson, “Reduced
896 order constrained optimization (ROCO): Clinical application to lung IMRT,” *Med. Phys.* **38**,
897 2731–2741, (2011).
- 898 ²⁵ Y. Yang and M. J. Rivard, “Dosimetric optimization of a conical breast brachytherapy applicator
899 for improved skin dose sparing,” *Med. Phys.* **37**, 5665–5671, (2010).
- 900 ²⁶ X. Zhang, J. Wang, and L. Xing, “Metal artifact reduction in x-ray computed tomography (CT)
901 by constrained optimization,” *Med. Phys.* **38**, 701–711, (2011).
- 902 ²⁷ D. Butnariu, R. Davidi, G. T. Herman, and I. G. Kazantsev, “Stable convergence behavior under
903 summable perturbations of a class of projection methods for convex feasibility and optimization
904 problems,” *IEEE J. Sel. Top. Sign. Process.* **1**, 540–547, (2007).
- 905 ²⁸ R. Davidi, G. T. Herman, and Y. Censor, “Perturbation-resilient block-iterative projection meth-
906 ods with application to image reconstruction from projections,” *Int. Trans. Oper. Res.* **16**, 505–
907 524, (2009).
- 908 ²⁹ Y. Censor, R. Davidi, and G. T. Herman, “Perturbation resilience and superiorization of iterative
909 algorithms,” *Inverse Probl.* **26**, 065008, (2010).
- 910 ³⁰ T. Nikazad, R. Davidi, and G. T. Herman, “Accelerated perturbation-resilient block-iterative
911 projection methods with application to image reconstruction,” *Inverse Probl.* **28**, 035005, (2012).
- 912 ³¹ G. T. Herman and R. Davidi, “Image reconstruction from a small number of projections,” *Inverse*
913 *Probl.* **24**, 045011, (2008).
- 914 ³² E. Garduño, R. Davidi, and G. T. Herman, “Reconstruction from a few projections by ℓ_1 -

- 915 minimization of the Haar transform,” *Inverse Probl.* **27**, 055006, (2011).
- 916 ³³ R. L. Rardin and R. Uzsoy, “Experimental evaluation of heuristic optimization algorithms: A
917 tutorial,” *J. Heuristics* **7**, 261–304, (2001).
- 918 ³⁴ L. Wernisch, S. Hery, and S. J. Wodak, “Automatic protein design with all atom force-fields by
919 exact and heuristic optimization,” *J. Mol. Biol.* **301**, 713–736, (2000).
- 920 ³⁵ S. H. Zanakakis and J. R. Evans, “Heuristic optimization - why, when, and how to use it,” *Interfaces*
921 **11**, 84–91, (1981).
- 922 ³⁶ G. T. Herman and W. Chen, “A fast algorithm for solving a linear feasibility problem with
923 application to intensity-modulated radiation therapy,” *Linear Algebra Appl.* **428**, 1207–1217,
924 (2008).
- 925 ³⁷ E. S. Helou Neto and Á. R. De Pierro, “Incremental subgradients for constrained convex opti-
926 mization: A unified framework and new methods,” *SIAM J. Optimiz.* **20**, 1547–1572, (2009).
- 927 ³⁸ E. S. Helou Neto and Á. R. De Pierro, “On perturbed steepest descent methods with inexact
928 line search for bilevel convex optimization,” *Optimization* **60**, 991–1008, (2011).
- 929 ³⁹ E. A. Nurminski, Envelope stepsize control for iterative algorithms based on Fejer processes with
930 attractants, *Optimiz. Method. Softw.* **25**, 97–108, (2010).
- 931 ⁴⁰ P. L. Combettes and J. Luo, “An adaptive level set method for nondifferentiable constrained
932 image recovery,” *IEEE Trans. Image Proc.* **11**, 1295–1304, (2002).
- 933 ⁴¹ P. L. Combettes and J.-C. Pesquet, “Image restoration subject to a total variation constraint,”
934 *IEEE Trans. Image Proc.* **13**, 1213–1222, (2004).
- 935 ⁴² E. Y. Sidky and X. Pan, “Image reconstruction in circular cone-beam computed tomography by
936 constrained, total-variation minimization,” *Phys. Med. Biol.* **53**, 4777–4807, (2008).
- 937 ⁴³ J. Bian, J. H. Siewerdsen, X. Han, E. Y. Sidky, J. L. Prince, C. A. Pelizzari and X. Pan,
938 “Evaluation of sparse-view reconstruction from flat-panel-detector cone-beam CT,” *Phys. Med.*
939 *Biol.* **55**, 6575–6599, (2010).
- 940 ⁴⁴ M. Defrise, C. Vanhove, and X. Liu, “An algorithm for total variation regularization in high-
941 dimensional linear problems,” *Inverse Probl.* **27**, 065002, (2011).
- 942 ⁴⁵ Y. Censor, W. Chen, P. L. Combettes, R. Davidi, and G. T. Herman, “On the effectiveness of
943 projection methods for convex feasibility problems with linear inequality constraints,” *Comput.*
944 *Optim. Appl.* **51**, 1065–1088, (2012).
- 945 ⁴⁶ J. Bioucas-Dias and M. Figueiredo, “A new TwIST: two-step iterative shrinkage/thresholding

- 946 algorithms for image restoration,” *IEEE Trans. Image Proc.* **16**, 2992–3004, (2007).
- 947 ⁴⁷ T. Goldstein and S. Osher, “The split Bregman method for L1 regularized problems,” *SIAM J.*
 948 *Imaging Sci.* **2**, 323–343, (2009).
- 949 ⁴⁸ L. A. Shepp and Y. Vardi, “Maximum likelihood reconstruction for emission tomography,” *IEEE*
 950 *Trans. Med. Imag.* **1**, 113–122. (1982).
- 951 ⁴⁹ E. Levitan and G. T. Herman, “A maximum a posteriori probability expectation maximization
 952 algorithm for image reconstruction in emission tomography,” *IEEE Trans. Med. Imag.* **6**:185–
 953 192, (1987).
- 954 ⁵⁰ W. Jin, Y. Censor and M. Jiang, “A heuristic superiorization-like approach to bioluminescence
 955 tomography,” in *Proceedings of the International Federation for Medical and Biological Engi-*
 956 *neering (IFMBE)* (Springer-Verlag, 2012), to appear.
- 957 ⁵¹ H. M. Hudson and R. S. Larkin, “Accelerated image reconstruction using ordered subsets of
 958 projection data,” *IEEE Trans. Med. Imag.* **13**, 601–609, (1994).
- 959 ⁵² T. Elfving, “Block-iterative methods for consistent and inconsistent linear equations,” *Numer.*
 960 *Math.* **35**, 1–12, (1980).
- 961 ⁵³ P. P. B. Eggermont, G. T. Herman, and A. Lent, “Iterative algorithms for large partitioned linear
 962 systems, with applications to image reconstruction,” *Linear Algebra Appl.* **40**, 37–67, (1981).
- 963 ⁵⁴ R. Aharoni and Y. Censor, “Block-iterative projection methods for parallel computation of so-
 964 lutions to convex feasibility problems,” *Linear Algebra Appl.* **120**, 165–175, (1989).
- 965 ⁵⁵ G. T. Herman, *Fundamentals of Computerized Tomography: Image Reconstruction from Projec-*
 966 *tions*, 2nd ed., Springer, 2009.
- 967 ⁵⁶ J. F. P. J. Abascal, J. Chamorro-Servent, J. Aguirre, S. Arridge, T. Correia, J. Ripoli, J.
 968 J. Vaquero, and M. Desco, “Fluorescence diffuse optical tomography using the split Bregman
 969 method,” *Med. Phys.* **38**, 6275–6284, (2011)
- 970 ⁵⁷ R. Davidi, G. T. Herman, and J. Klukowska, *SNARK09: A Programming System for the Re-*
 971 *construction of 2D Images from 1D Projections*, <http://www.snark09.com>, 2009.
- 972 ⁵⁸ G. T. Herman and L. B. Meyer, “Algebraic reconstruction techniques can be made computa-
 973 tionally efficient,” *IEEE Trans. Med. Imag.* **12**, 600–609, (1993).
- 974 ⁵⁹ W. Zbijewski and F. J. Beekman, “Characterization and suppression of edge and aliasing artefacts
 975 in iterative x-ray CT reconstruction,” *Phys. Med. Biol.* **49**, 145–157, (2004).